THE RESPONSE OF OPTICAL ARRAY SPECTROMETERS TO ICE AND SNOW: A STUDY OF PROBE SIZE TO CRYSTAL MASS RELATIONSHIPS

Robert G. Knollenberg

Particle Measuring Systems, Incorporated

Prepared for:

Air Force Cambridge Research Laboratories

8 September 1975

042063

AFCRL-TR-75-0494

THE RESPONSE OF OPTICAL ARRAY SPECTROMETERS TO ICE AND SNOW: A STUDY OF PROBE SIZE TO CRYSTAL MASS RELATIONSHIPS

Dr. Robert G. Knollenberg

Particle Measuring Systems, Inc.,
1855 South 57th Court
Boulder, Colorado 80301

September 8, 1975

SCIENTIFIC REPORT NO.1
SCI75C0141-9875-001

This Research was Sponsored by the Space and Missile Systems Organization

AIR FORCE CAMBRIDGE RESEARCH LABORATORIES
AIR FORCE SYSTEMS COMMAND
UNITED STATES AIR FORCE
HANSCOM AFB, MASSACHUSETTS 01731

79

Qualified Requestors may obtain additional copies from the Defense Documentation Center. All others should apply to the National Technical Information Service.

SECURITY CLASSIFICATION OF THIS PAGE (When Data Entered)

REPORT DOCUMENTATION PAGE

READ INSTRUCTIONS BEFORE COMPLETING FORM

1. REPORT NUMBER: AFCRL-TR-75-0494	2. GOVT ACCESSION NO.
3. RECIPIENT'S CATALOG NUMBER	
4. TITLE (and Subtitle): "Response of Optical Array Spectrometers to Ice and Snow: A Study of Probe Size to Crystal Mass Relationships"	5. TYPE OF REPORT & PERIOD COVERED: Scientific Report No. 1, 14FEB75 - 15AUG75
	6. PERFORMING ORG. REPORT NUMBER
7. AUTHOR(s): Dr. Robert G. Knollenberg	8. CONTRACT OR GRANT NUMBER(s): F19628-75-C-0141
9. PERFORMING ORGANIZATION NAME AND ADDRESS: Particle Measuring Systems, Inc., 1855 South 57th Court, Boulder, Colorado 80301	10. PROGRAM ELEMENT, PROJECT, TASK AREA & WORK UNIT NUMBERS: 63311F, 627A0001
11. CONTROLLING OFFICE NAME AND ADDRESS: Air Force Cambridge Research Laboratories, Hanscom AFB, Massachusetts 01731, Contract Monitor, Wilbur H. Paulsen/LYC	12. REPORT DATE: September 8, 1975
	13. NUMBER OF PAGES: 79
14. MONITORING AGENCY NAME & ADDRESS (if different from Controlling Office)	15. SECURITY CLASS. (of this report): Unclassified
	15a. DECLASSIFICATION DOWNGRADING SCHEDULE

16. DISTRIBUTION STATEMENT (of this Report)

Approved for public release; distribution unlimited

17. DISTRIBUTION STATEMENT (of the abstract entered in Block 20, if different from Report)

18. SUPPLEMENTARY NOTES

This research was sponsored by Space and Missile Systems Organization

19. KEY WORDS (Continue on reverse side if necessary and identify by block number)

Probe Response
Snow Crystals

20. ABSTRACT (Continue on reverse side if necessary and identify by block number)

This report is a summary of work performed by Particle Measuring Systems, Inc., to study the response of Optical Array Spectrometers to ice and snow crystals. The principle objective of this study was to perform laboratory, field and theoretical studies to establish more appropriate optical array probe particle size-to-mass relationships. The studies involved both 1-D and 2-D optical array spectrometers. The following report briefly describes the work performed and the results. The sections are not necessarily

DD FORM 1 JAN 73 1473 EDITION OF 1 NOV 65 IS OBSOLETE

Unclassified

SECURITY CLASSIFICATION OF THIS PAGE (When Data Entered)

organized in the chronology that they were performed. While it was intended that the theoretical work might be performed prior to field studies it was necessary to modify theoretical models based upon field observations. In many cases, phases of this work proceeded essentially in parallel with considerable readjustment upon integrating all phases of work.

TABLE OF CONTENTS

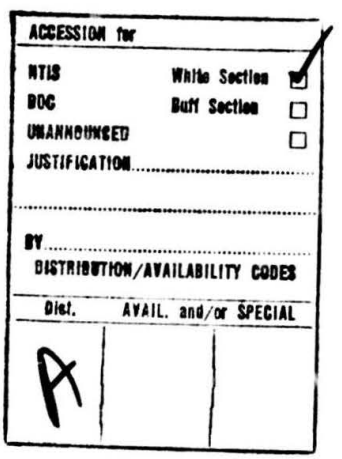

LIST OF FIGURES

List of Figures (con't)

List of Figures (con't)

LIST OF TABLES

1.0 INTRODUCTION

• This report is a summary of work performed by PMS to study the response of Optical Array Spectrometers to ice and snow crystals. A principle goal of these efforts was the determination of more appropriate probe size to snow crystal mass relationships.

The Optical Array Spectrometer is an instrument developed by Knollenberg(1969, 1970, 1972)and manufactured by Particle Measuring Systems,Inc., of Boulder, Colorado. The basic technique of the Optical Array Spectrometer utilizes a laser to illuminate particles passing through the object plane of an imaging system. The particle shadows are imaged onto a photodiode array and are sized as an integral number of occulted elements. The particle size is determined by the size of the photodiode elements and the magnification of the imaging system. While the instrument avoids many of the uncertainties of other techniques, certain systematic errors can result (see Knollenberg 1972). In general, the instrument performs as a quantizing or digitizing device responding to projected particle dimension; however, at the limit of resolution the percentage area of any diode element that is occulted is the limiting factor and introduces a roundoff error in the sizing process. Because of the area dependence. the sizing accuracy varies as a function of particle position and shape. For instance, measurements of snow crystal size spectra have recently shown that there is a systematic tendency for underestimating the mass of snow crystals from sizes measured with Optical Array Spectrometers. In particular, the ice water content (IWC) computed from data taken from AFCRL C-130 aircraft during the past year at Wallops Island have underestimated IWC by a

factor of five when compared to Wallops Island radar[1]. It is also relevant that the greatest disagreement between a particular Optical Array Probe (OAP) integrated IWC and that from radar data is in the region of predominant "a" axis crystal growth (planar growth is along the "a" axis and columnar growth is along the "c" axis). On the other hand, data taken during the same flights at the lower levels in rain and in the upper cirriform clouds give much better agreement and, in fact, correlations are as good as might be expected.

The above problem outlined, while showing a disagreement, has one encouraging characteristic: The error is a systematic error with OAP measured IWC consistently less than radar IWC. There was little doubt that the problem primarily lay in the mass assigned to the probe size. It was expected that this was a two part error:

1) The probe undersizes the ice crystal
2) The snow crystal mass is greater than that assigned to the particle size.

A third factor, namely the loss of measurement of crystals larger than 4.5 mm, also contributes to less OAP IWC but the discrepancy is apparent even when no crystals larger than 4.5 mm are present. The above problems are greatly reduced with spherical water drops (an ideal shape for probe response). In cirriform clouds the particle shape is more uniform in habit and

---

1 Radar, in general, respond to the 6th moment of particle radius, i.e., (Z) or (mass^2). It is understood that the IWC is not extractable from radar Z without a prior knowledge of particle size or an assumed Z-M relationship. The Z values are ultimately what is compared and for the purposes of this exercise the probe IWC may be interpreted as comparable to $\sqrt{Z}$ (radar).

density which when coupled with the data available from simultaneous snow crystal mass measurements during probe operation has resulted in less discrepancy.

From the above background, it was apparent that additional studies were required to compare OAP measured snow crystal size with the equivalent crystal melted diameter over a broader range of crystal habit. The objective of this study was to provide laboratory, field and theoretical studies to establish more appropriate OAP particle size-to-mass relationships. The studies involved both 1-D and 2-D Optical Array Spectrometers. The following sections briefly describe the work performed and the results. The sections are not necessarily organized in the chronology that they were performed. While it was intended that the theoretical work might be performed prior to field studies it was necessary to modify theoretical models based upon field observations. In many cases phases of this work proceeded essentially in parallel with considerable readjustment upon integrating all phases of work.

2.0 THEORETICAL STUDIES: PROBE RESPONSE TO SPHERICAL PARTICLES AND SNOW CRYSTALS OF VARIOUS HABIT

This portion of the work involved the computed response of OAP probes to snow crystals of differing size and crystalline habit. The computations were performed primarily for single crystals with emphasis on forms with planar growth in the "a" axis. It is an observed fact that snow crystals fall with preferential orientation in the atmosphere. The crystals invariably orient with their largest cross sectional area in the horizontal plane (orthogonal to drag and gravitational forces). Since the OAP probes are normally oriented vertically, this is the dimension that is measured.

The effect of the size (area) of the array elements is critical to avoid undersizing or even missing the open structure of snow crystals, particularly those of the dendrite family. The first production OAPs had arrays whose elements were elongated, requiring that snow crystal shadows be approximately twice as large as the element spacing to register (see Figure 1). The branches of dendrites are quite thin when compared to their overall crystal diameter. Unless the branches are as wide as one element, they will not be seen by the OAP. One likely result would be that the probe would effectively "disarm" these crystals when sizing. Likewise, crystals of the needle family are very difficult for the OAP to respond to until the width approximates an array element in size. The finer features of all crystals would appear to be often missed.

With arrays of more ideal element geometry (circular) the problem is greatly reduced, but still exists (see Figure 2).

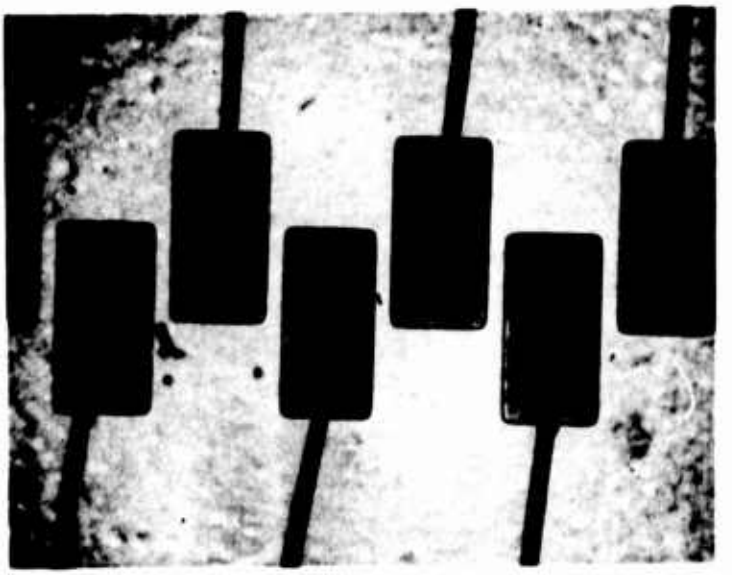

Photomicrograph of Array Element Geometry Used in First Production OAPs. Active area includes all dark shaded area except that covered by 1 1/2 mil bonding wires.

FIGURE 1

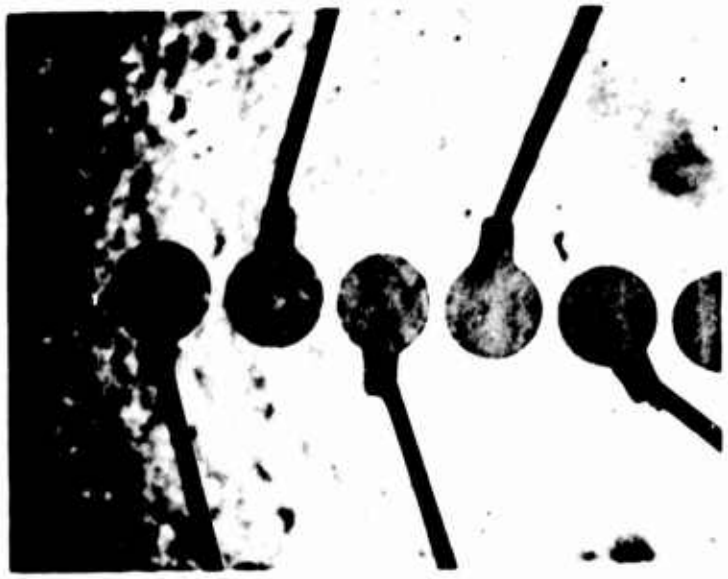

Photomicrograph of Array Currently Used in OAPs. Elements have circular geometry with small tab used for wire bonding. Total active area is less than half that depicted in Figure 1 for the previous rectangular element arrays.

FIGURE 2

Since the newer arrays (and all replacement arrays) have the preferred circular element geometry, they are of primary importance; however, these studies will include both array geometries. While this part of the study provides OAP theoretical response functions to various crystalline forms, because of the tremendous natural variation in habit and the scaling of crystal size within each type, only ideal (average) crystalline types could be used. These are listed in Table 1 along with the crystallographic symbology of Magono & Lee, 1966.

The purpose of this study was to predict the sizing accuracy of an OAP to these habit variations. The method by which this was accomplished involved several steps. First the crystallographic habit was studied from field data to establish shape factors or the "average" snow crystal of each type. For example, a plate with dendritic extensions has a certain plate dimension within the entire crystal. The relative size of this plate has a marked effect on the calculated response. Likewise, a stellar crystal is extremely sensitive to the width of it's branches. The real "average" crystal types are shown in Figure 3. The "average" symmetry was established through detailed analysis of collected snow crystals. In fact, the small snow and large snow classes involved using shapes of many snow crystal samples, computing the response function individually, and then averaging over many of these response functions. The crystal shape for large and small snow is only symbolic in this case.

The array geometries given in Figures 1 and 2 are also

HABIT	CLASSIFICATION CODE
1. Spheres	
2. Plates	P1a
3. Daisy	R4a
4. Branched Dendrite	P1g
5. Stellar Dendrite	P1e
6. Column 4:1 Aspect Ratio	C1c
7. Needle 7.5:1 Aspect Ratio	N1a
8. Stellar with End Plates	P1h
9. Rosettes	C2b
10. Sector Plate	P1b
11. Large and Small Snow	I1

See Magono and Lee (1966) for a general explanation of crystal classification

Snow Crystals Theoretically Studied

TABLE 1

IDEAL (AVERAGE) CRYSTAL MODELS FOR PROBE RESPONSE COMPUTATIONS

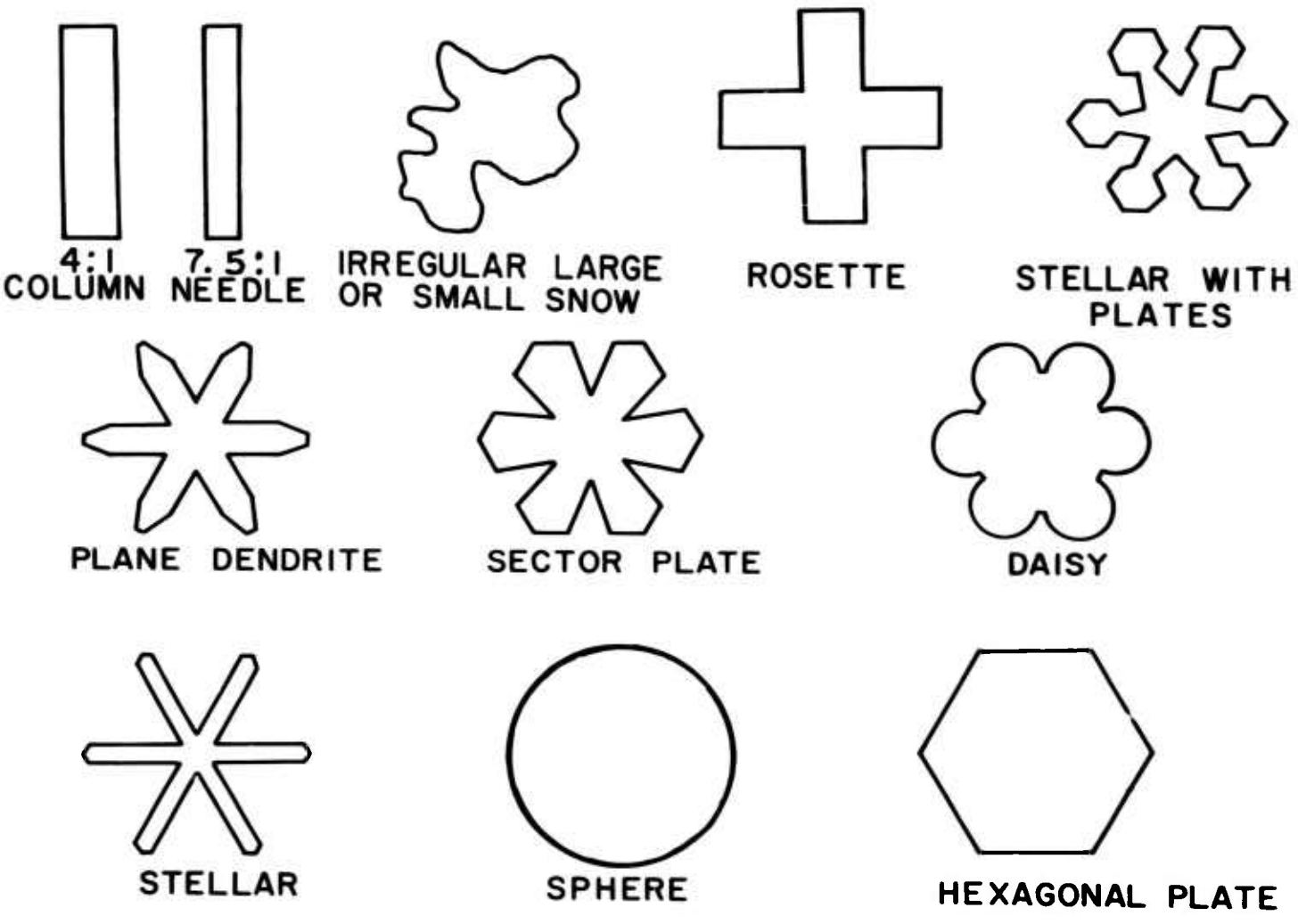

FIGURE 3

RECTANGULAR DETECTOR ARRAY RESOLUTION GRIDS

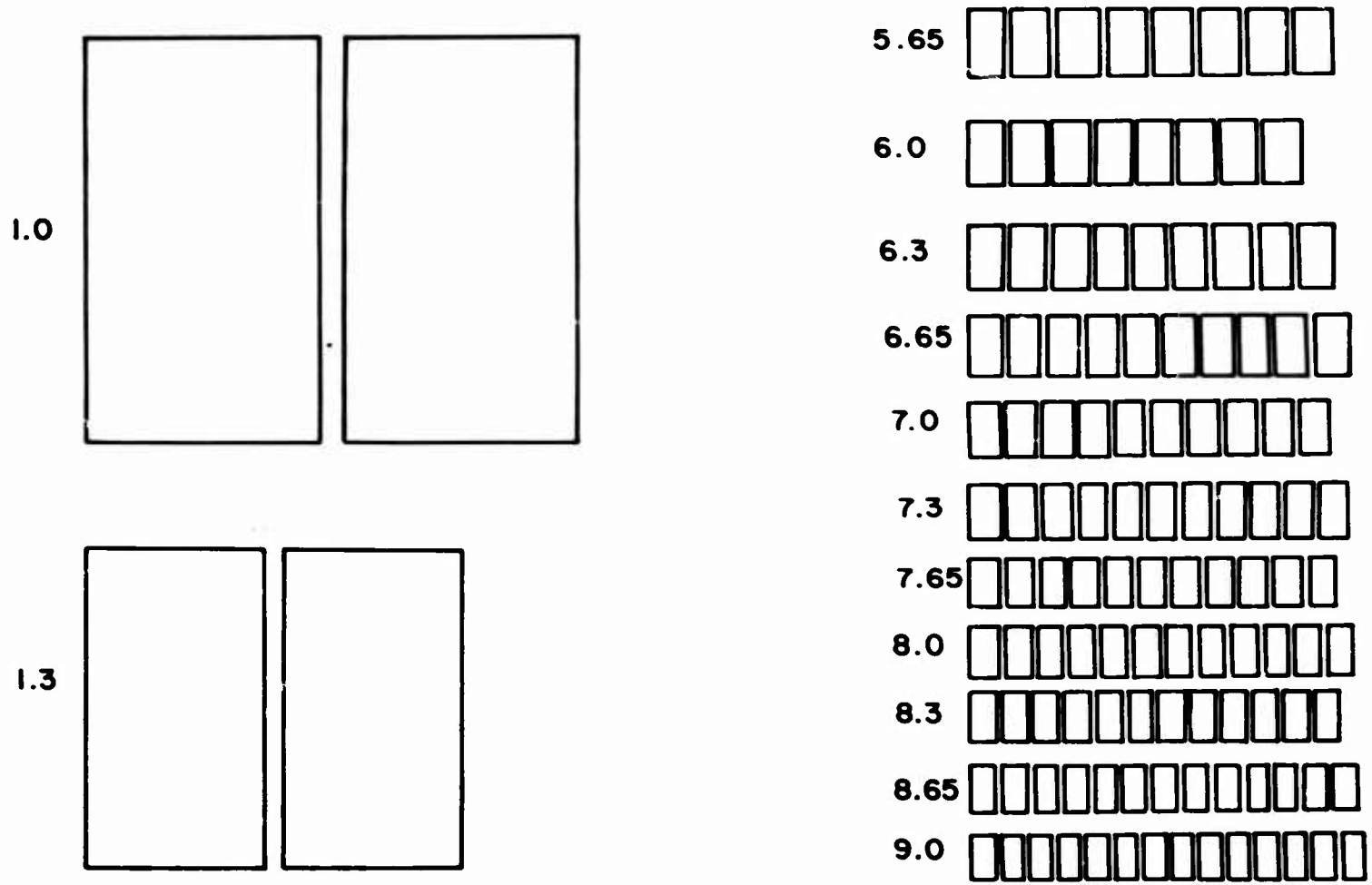

FIGURE 4

ROUND DETECTOR ARRAY RESOLUTION GRIDS

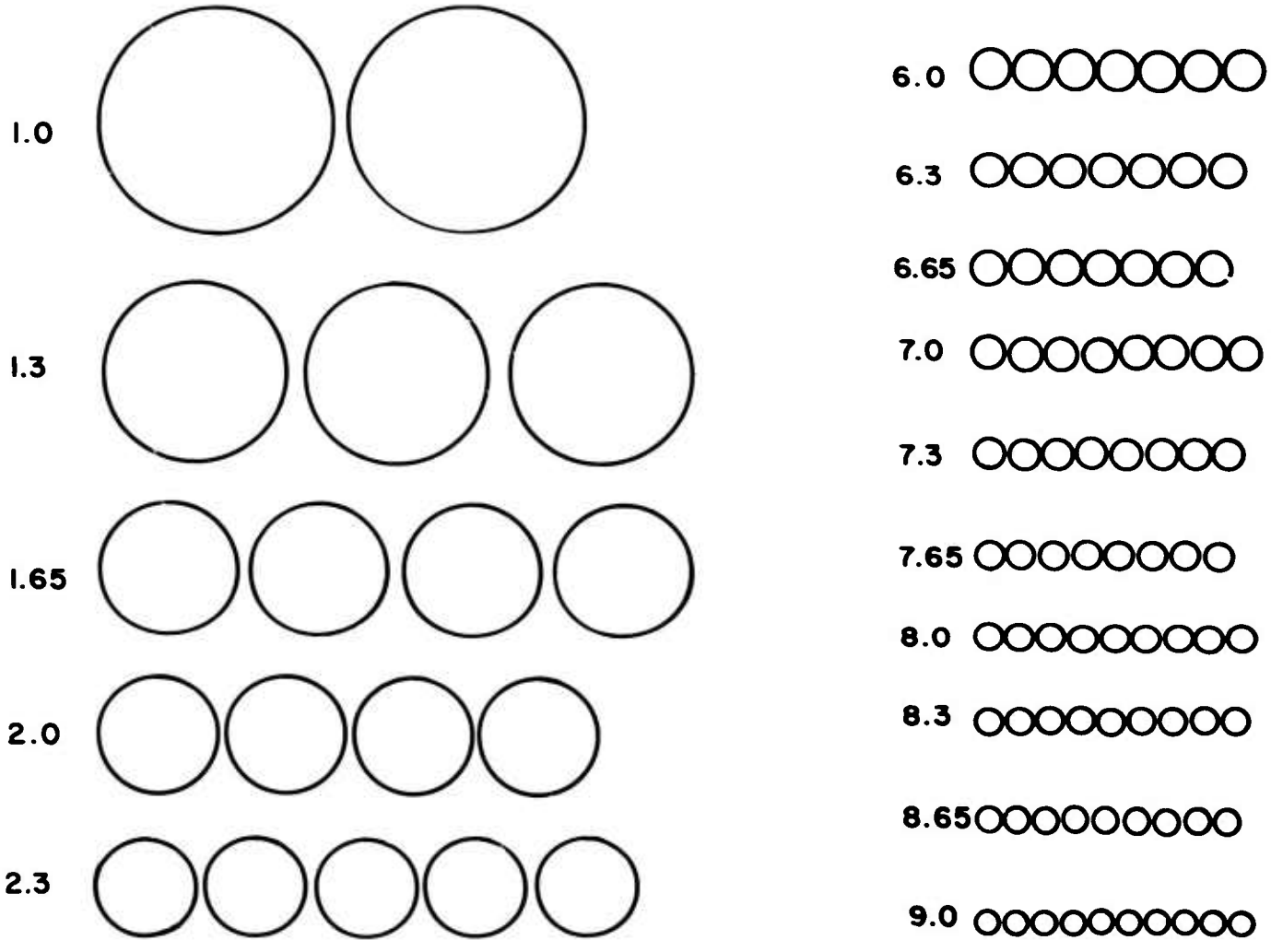

FIGURE 5

depicted in Figures 4 and 5 for various resolution levels to determine the response of either array geometery to a given crystal shape. It is necessary to determine how many array elements would be occulted during a crystal shadow's (actually the geometric shadow of the crystal) transit across the array. Because of the 50% threshold level used to define occultation conditions,the geometric shadow need only cover half an array element to result in occultation. Since the probability of occultation of any one diode element depends on the orientation of the crystal and its registration with respect to that element, a sufficient number of permutations of the particle image have to be tested to establish the "average" response for a given ratio of array element size (actually element spacing) to crystal size. This ratio is varied by changing the array element size (spacing) rather than the crystal image size during these tests.

The result of such measurements can be plotted as a set of curves of the type shown in Figure 6. The ordinate is the percent probability of a spherical image being measured. The abcissa is the sphere size. There are shown a series of triangular curves which are the envelopes of the percentage of particle sizes which are sized as a given probe size (shown numerically at the top of the triangles a- a certain number of occulted elements). In the example shown for a spherical particle, the threshold particle size has to be 0.71 of the element spacing to be seen (result in occultation) fifty percent of the time. A particle shadow of diameter 1.25 times the element spacing has a 100% probability of occulting one element during transit. If it is slightly larger it must have a measureable probability of occulting two elements and the probability of being sized as one element correspondingly decreases. The 100% probability

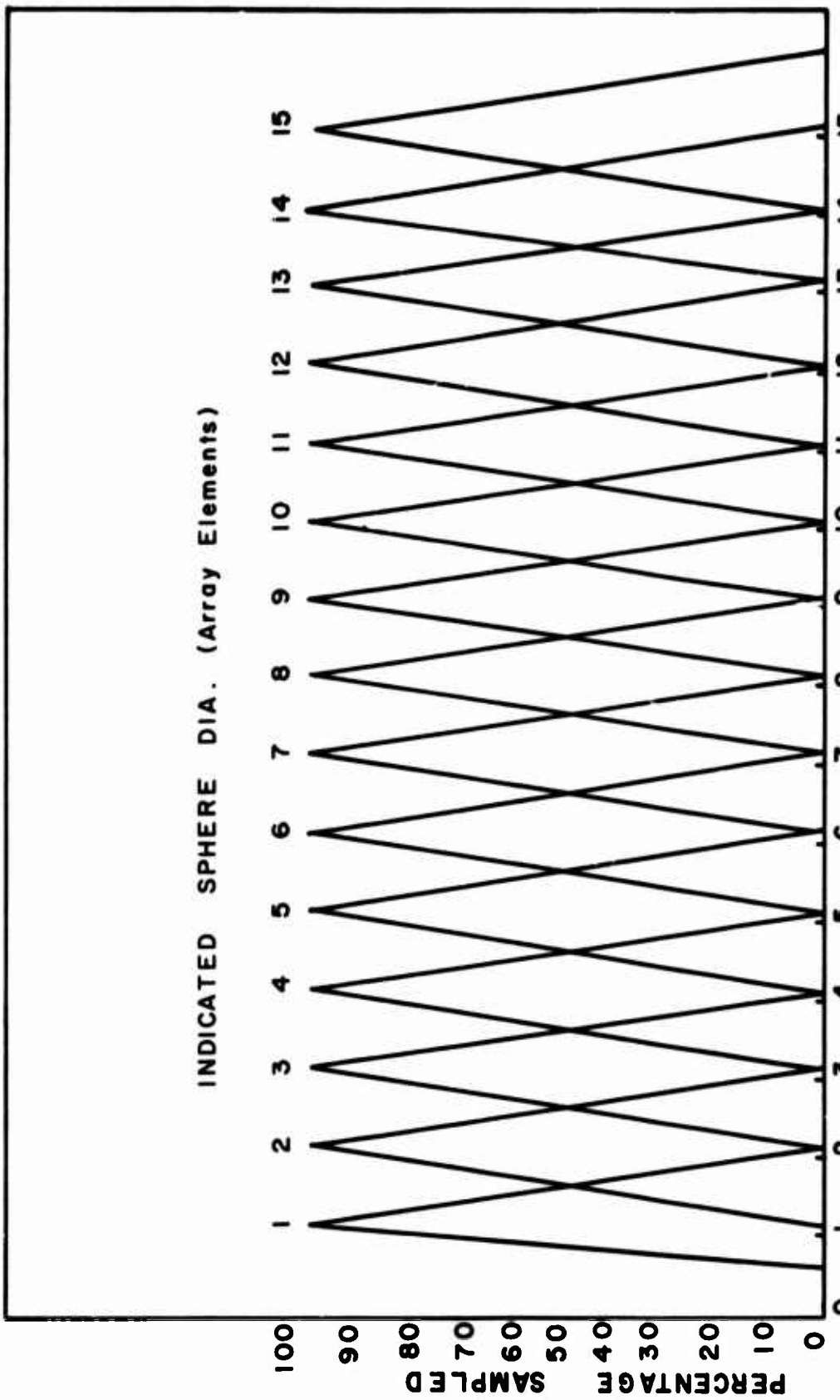
SPHERE PROBE RESPONSE GRAPH
PERCENTAGE SAMPLED
0
10
20
30
40
50
60
70
80
90
100
INDICATED SPHERE DIA. (Array Elements)
0
1
2
3
4
5
6
7
8
9
10
11
12
13
14
15
SPHERE DIA. (Array Elements)

FIGURE 6

size should be considered as the true size class size. The true size class interval is defined by the intersection of two triangles at the 50% probability points.

The first size class is peculiar in that no smaller class exists for which the size is rounded down to. There is a certain threshold size above which a particle has a certain probability of being seen during transit. This threshold for detection has also been established. For the case just described with the 50% probability being 0.71 the corresponding threshold is 0.63. The essential information given by the "primitive" probability curves of the type shown in Figure 6 are replotted in Figures 7 through 26. There are two sets of figures;eleven for round and nine for rectangular detectors. The curves show the size intervals for each crystal diameter corresponding to the indicated snowcrystal diameter (number of occulted array elements).

In order to use the curves for a given crystal shape, it is only necessary to know the actual probe array element spacing (e.g. 20u for a Model 200X and 300u for a Model 200Y OAP probe) and multiply it times the size class interval numerical values to compute actual crystal size. For instance looking at Figure 11, an indicated branched dendrite size of 10 would correspond to a real crystal size of 211-231 microns rather than 20 X 10 or 200 microns.

The theoretical response functions have noticeably greater correction factors for the first few channels than higher channels. Note that for the spherical particle size class 15 covers from 14.52 to 15.50 with its computed true size of 15.01 or less than 1% statistical error while size

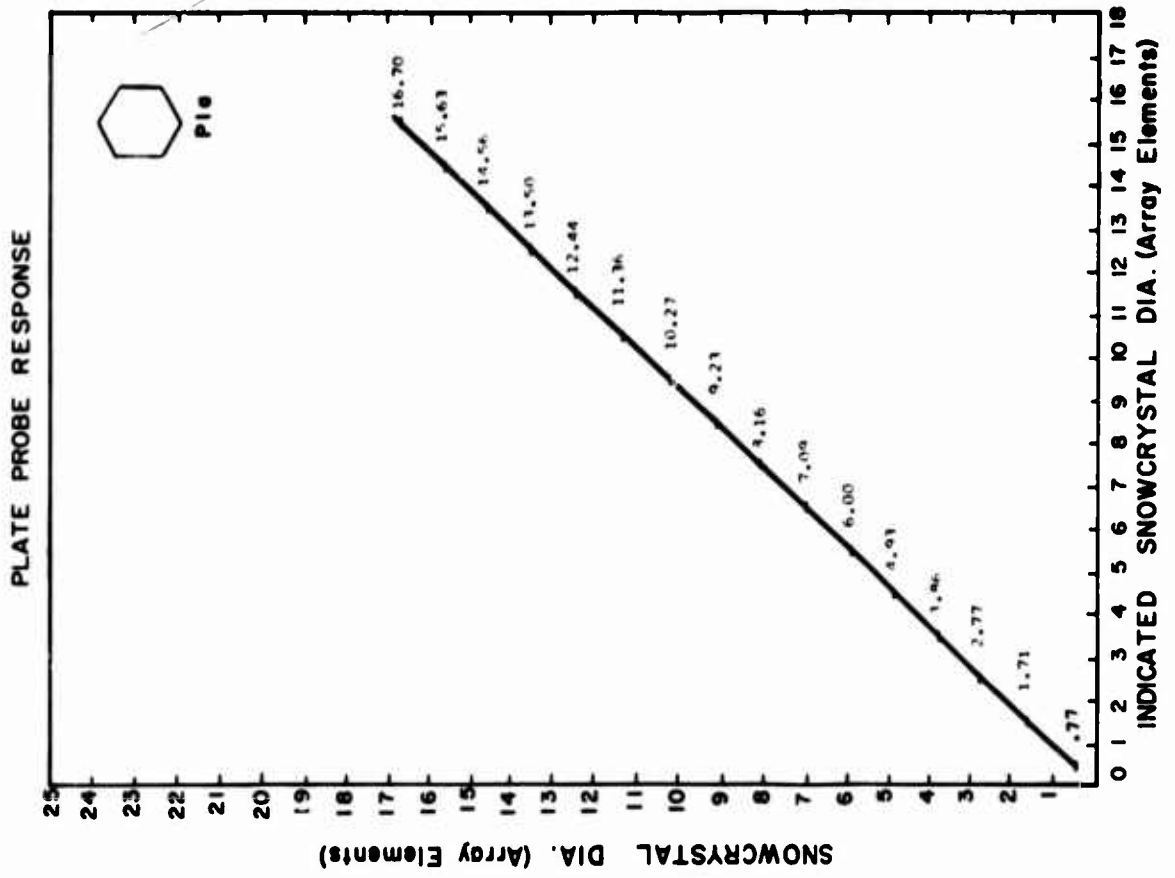

FIGURE 8

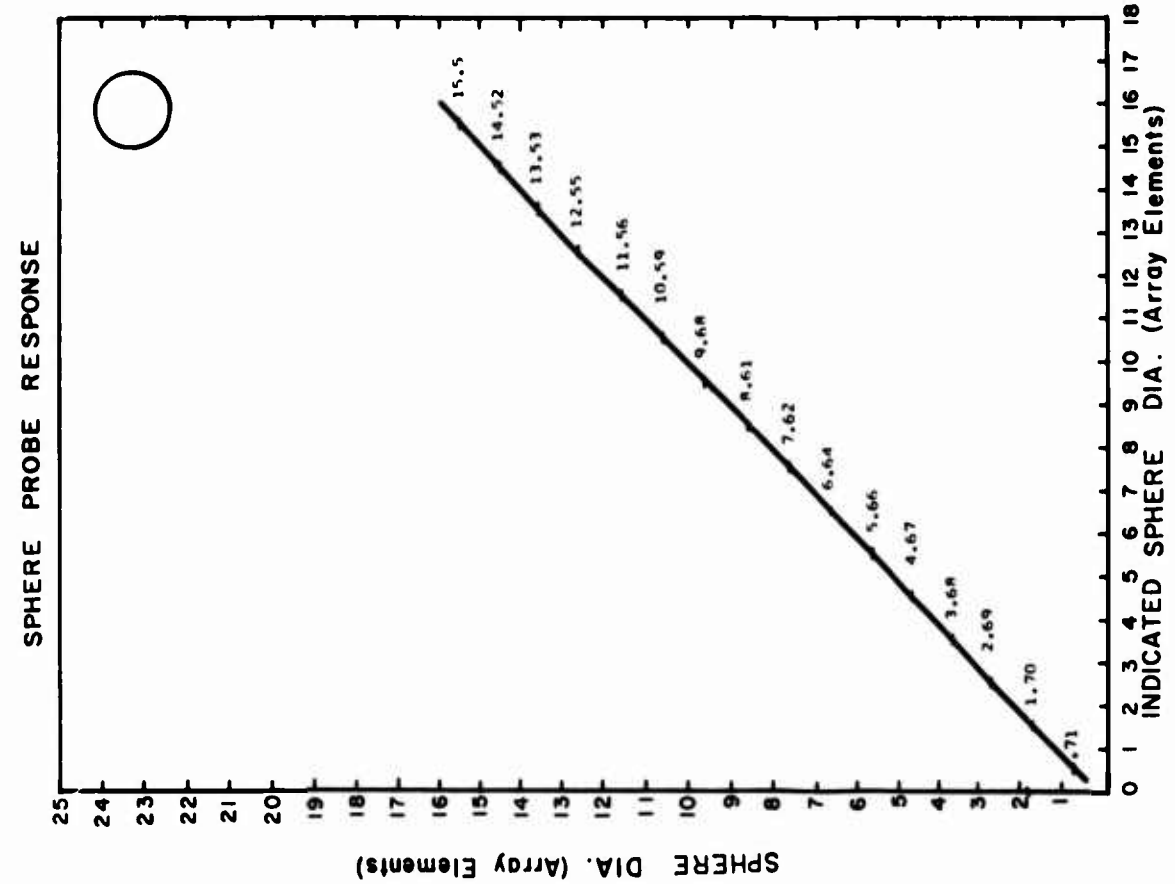

FIGURE 7

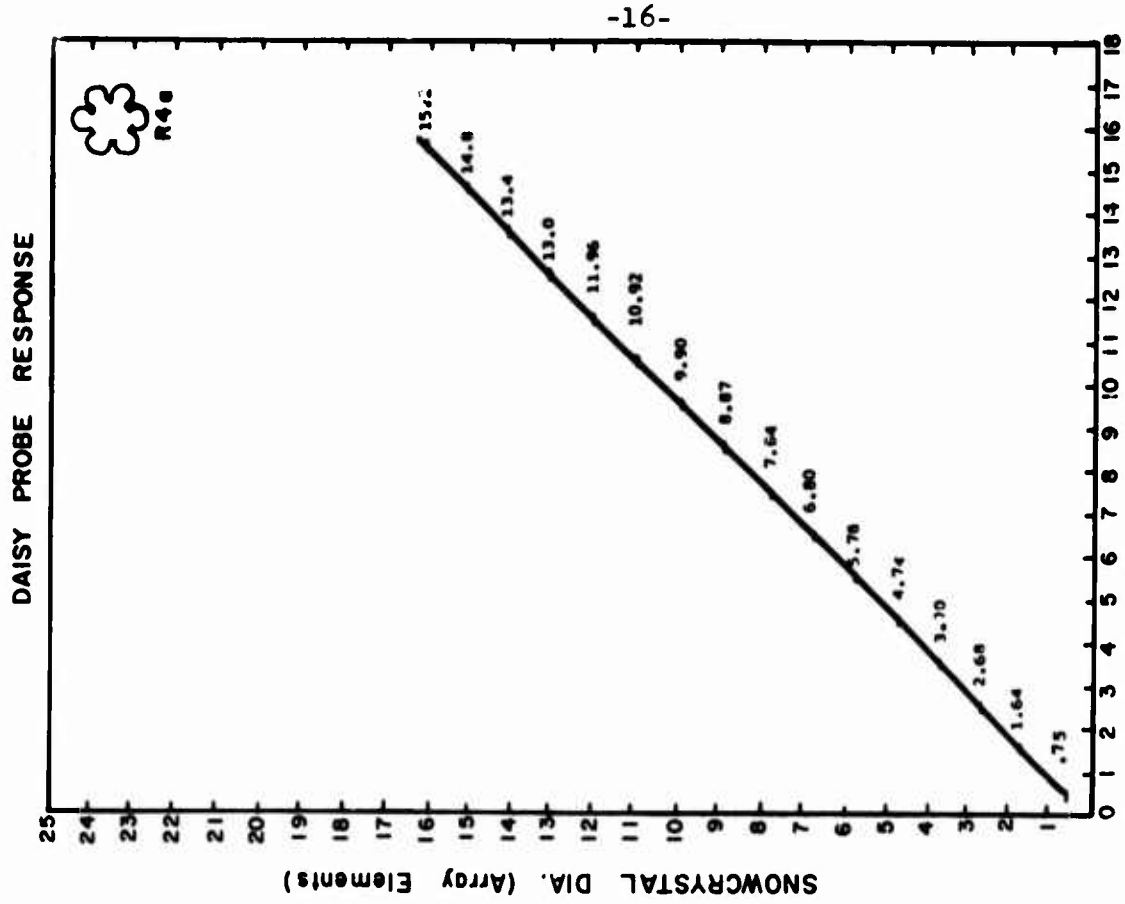

FIGURE 9

FIGURE 10

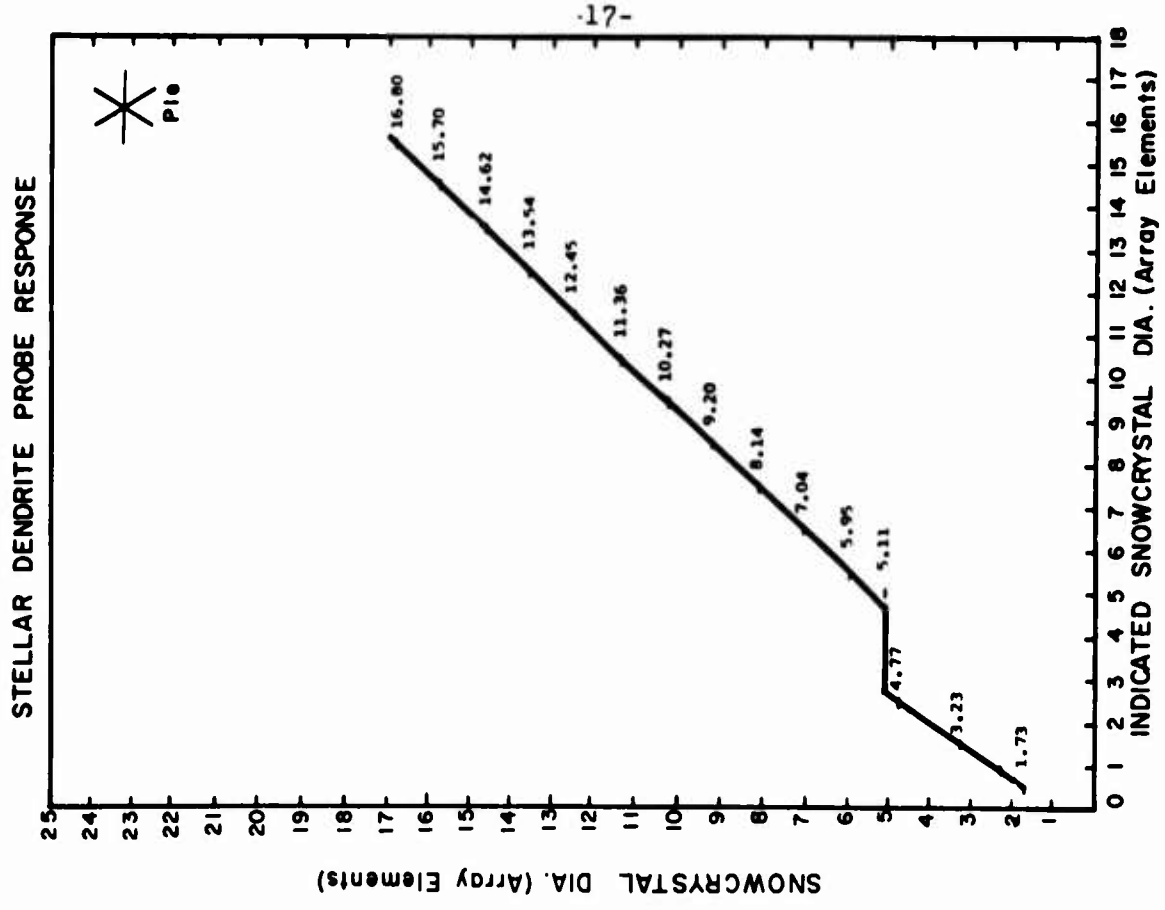

FIGURE 12

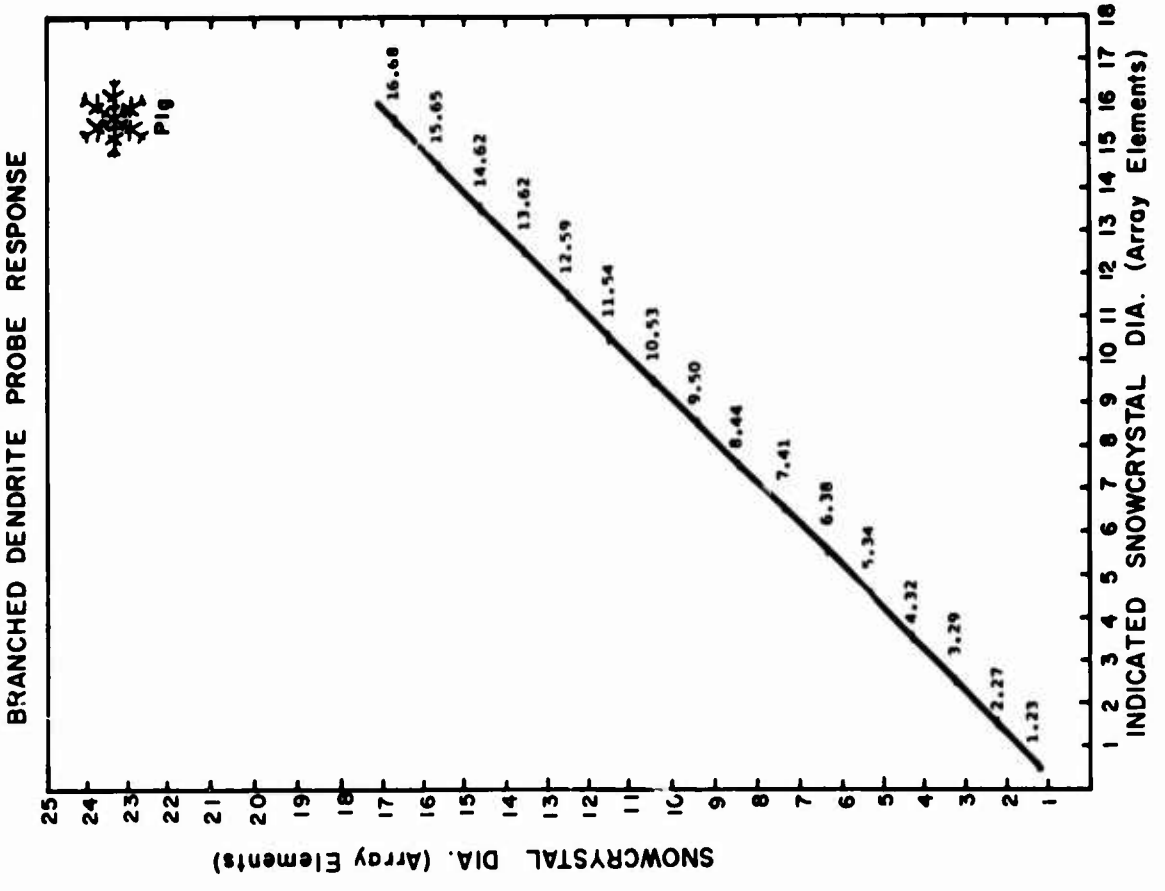

FIGURE 11

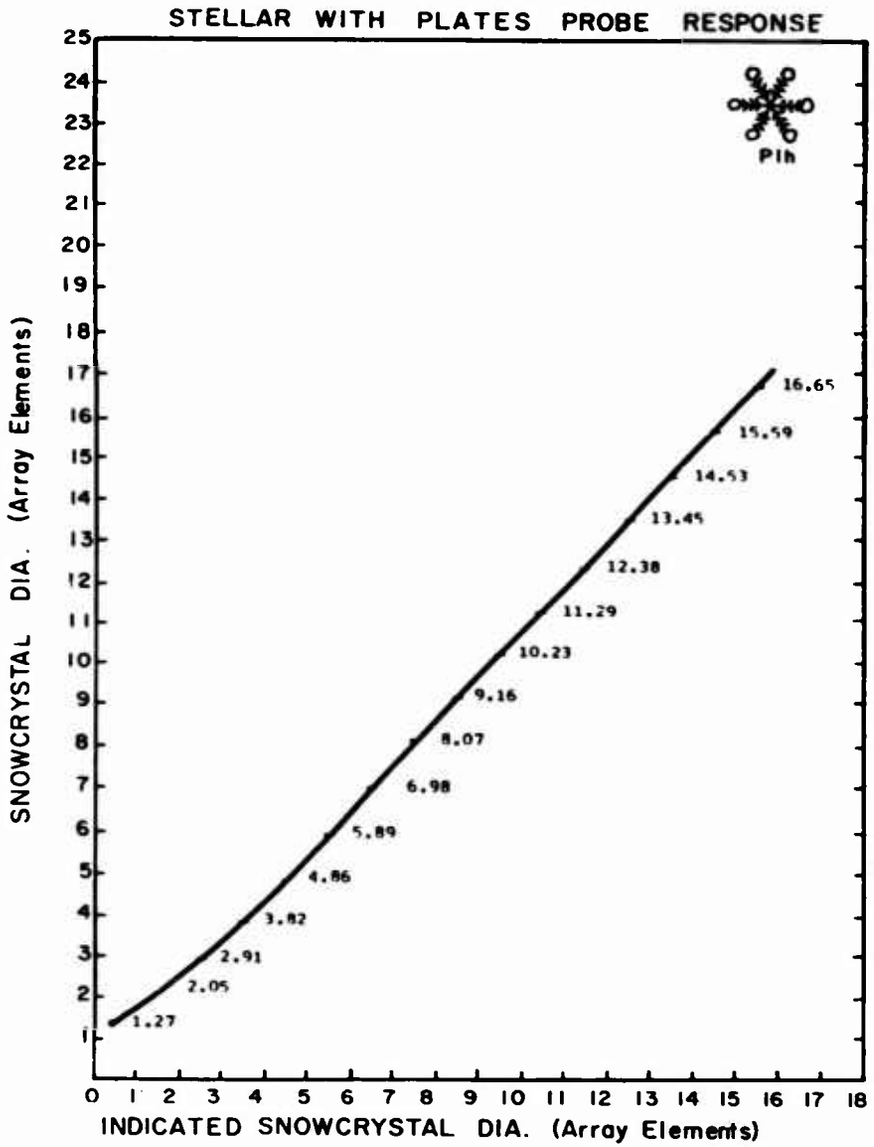

FIGURE 13

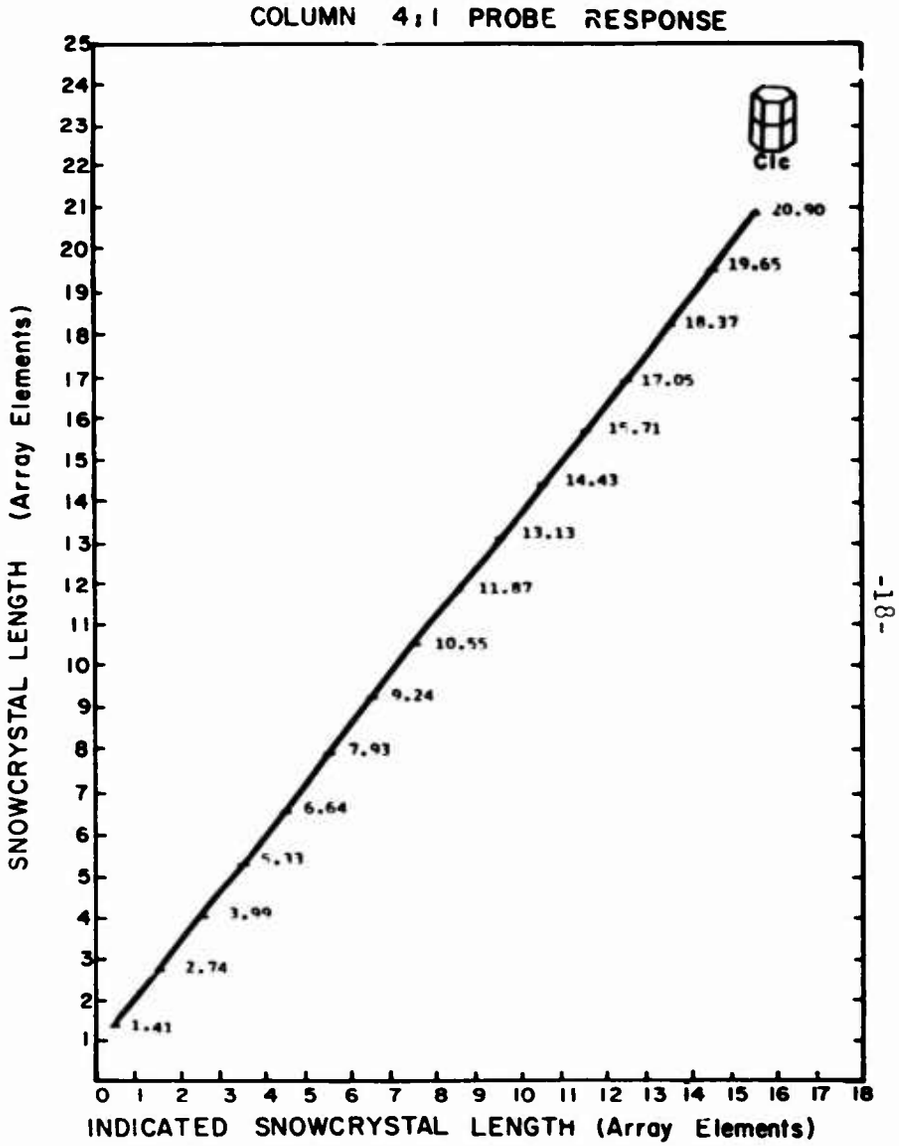

FIGURE 14

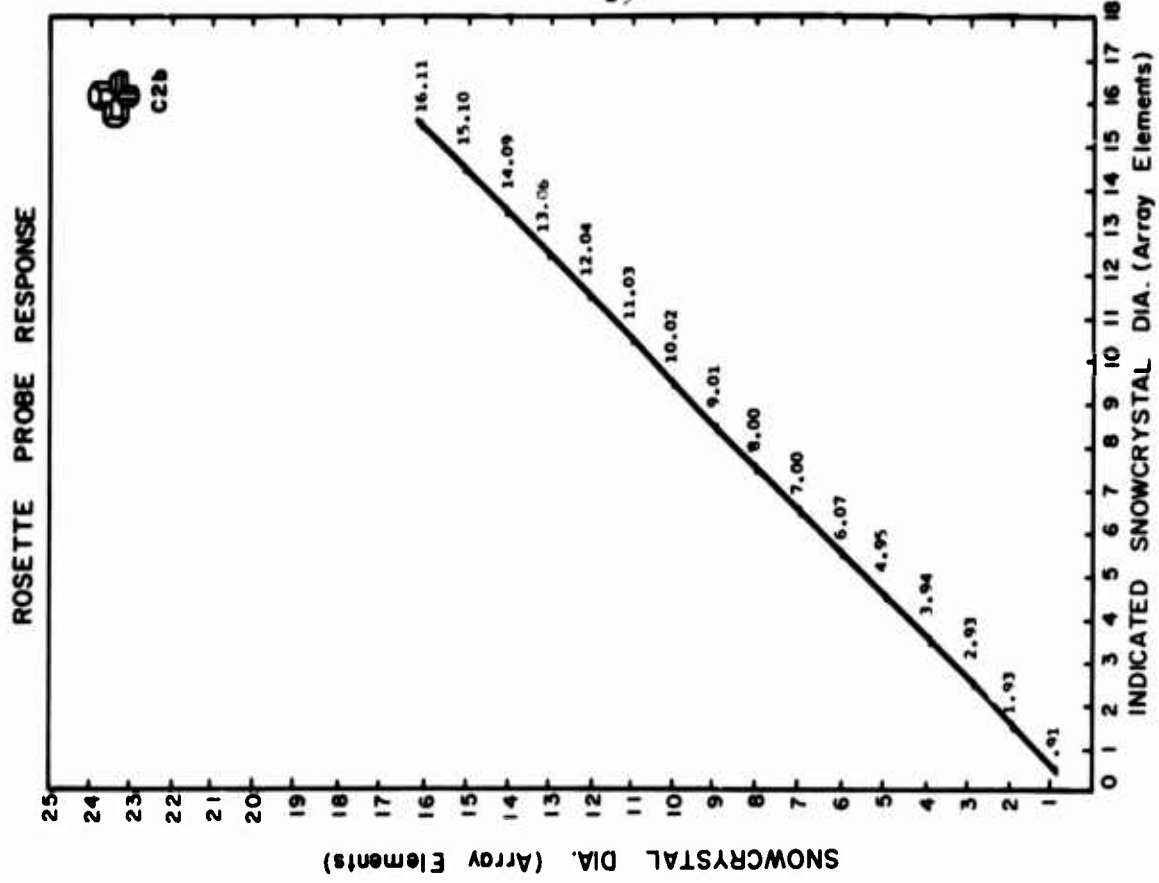

FIGURE 16

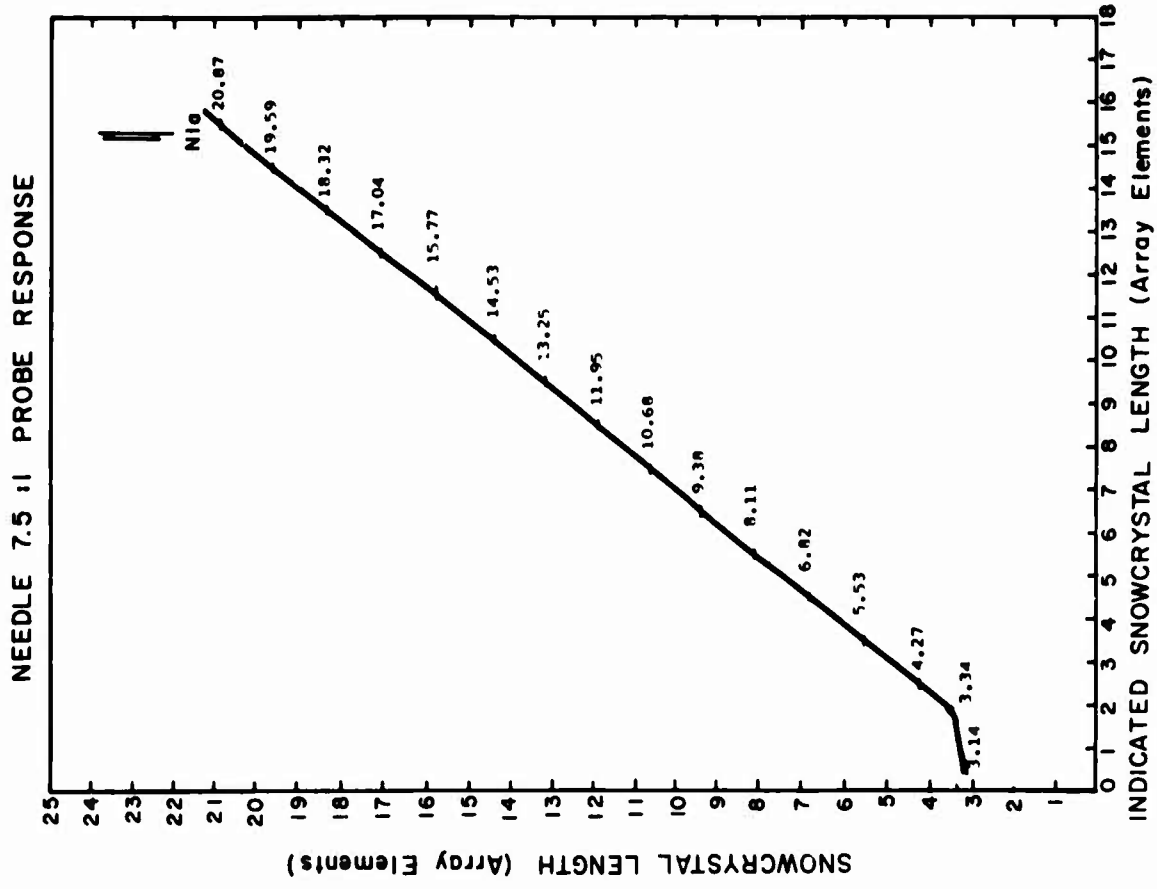

FIGURE 15

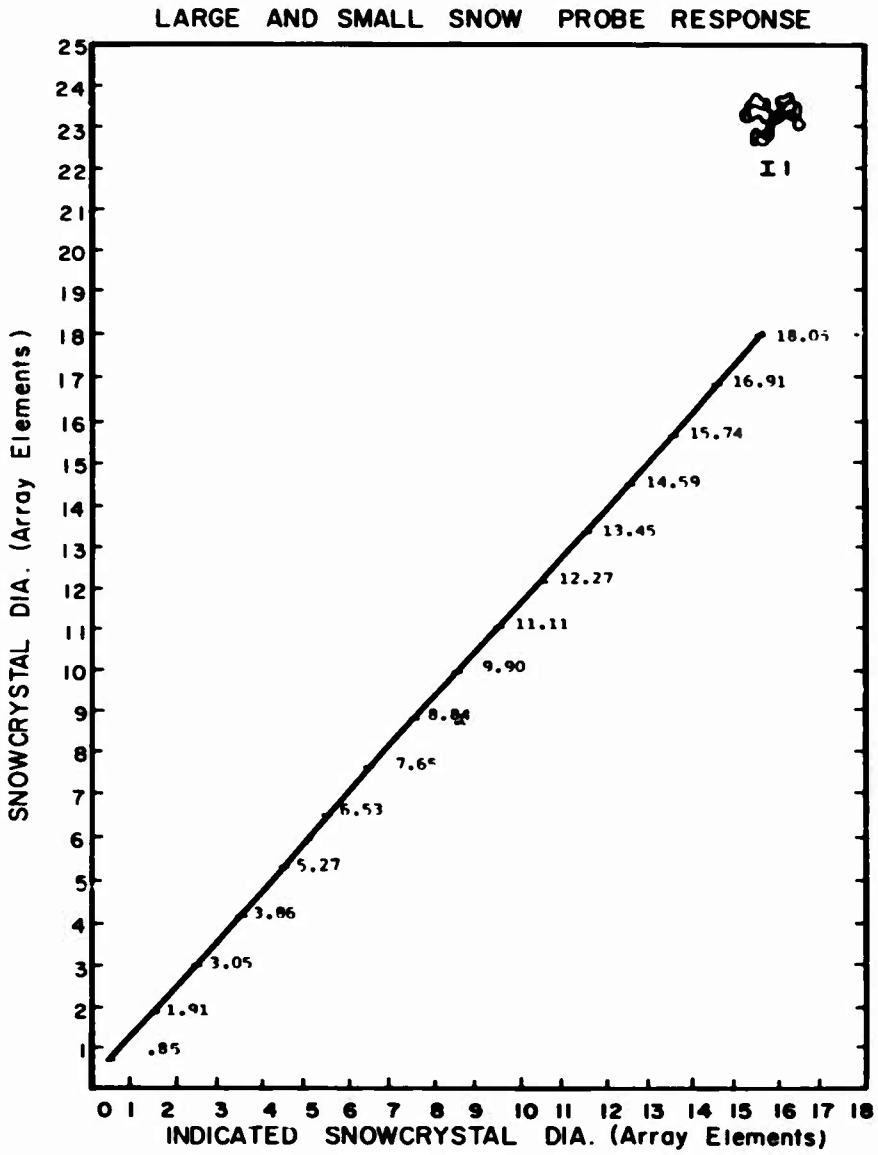

FIGURE 17

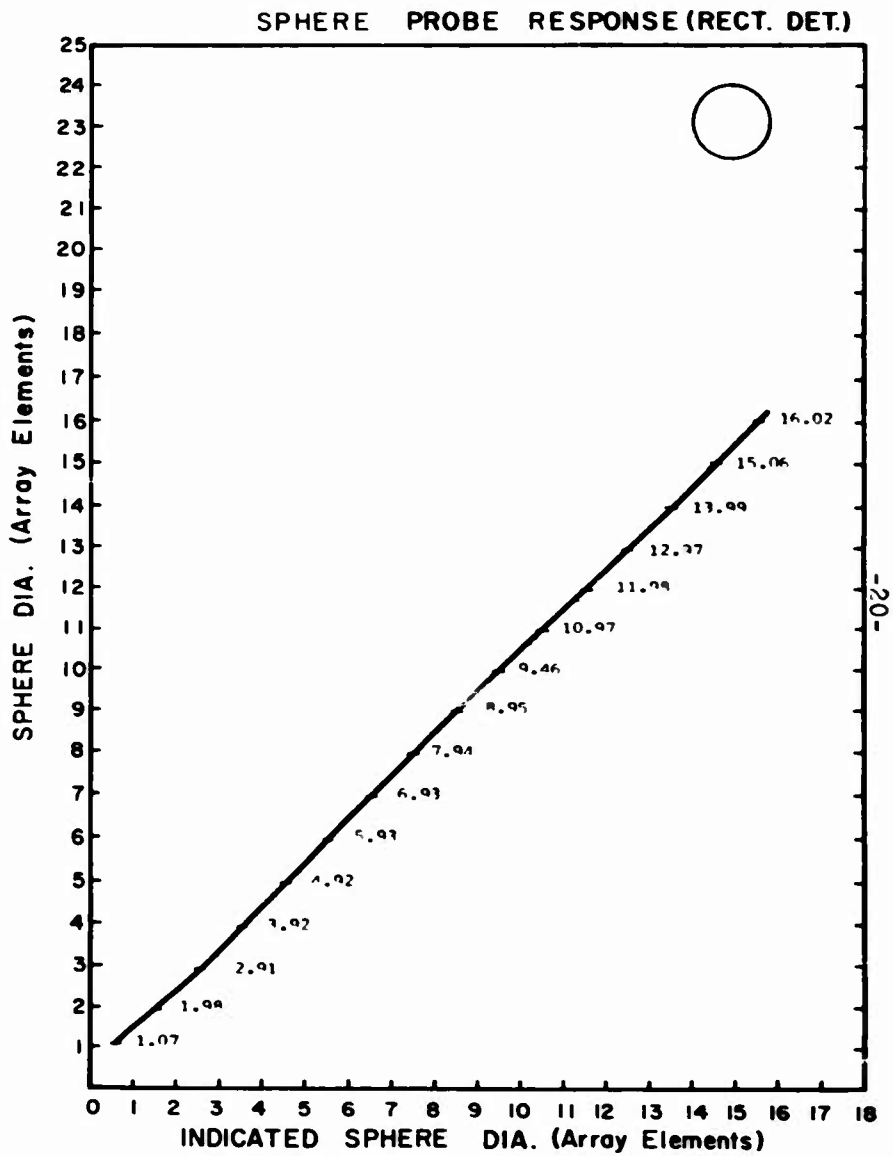

FIGURE 18

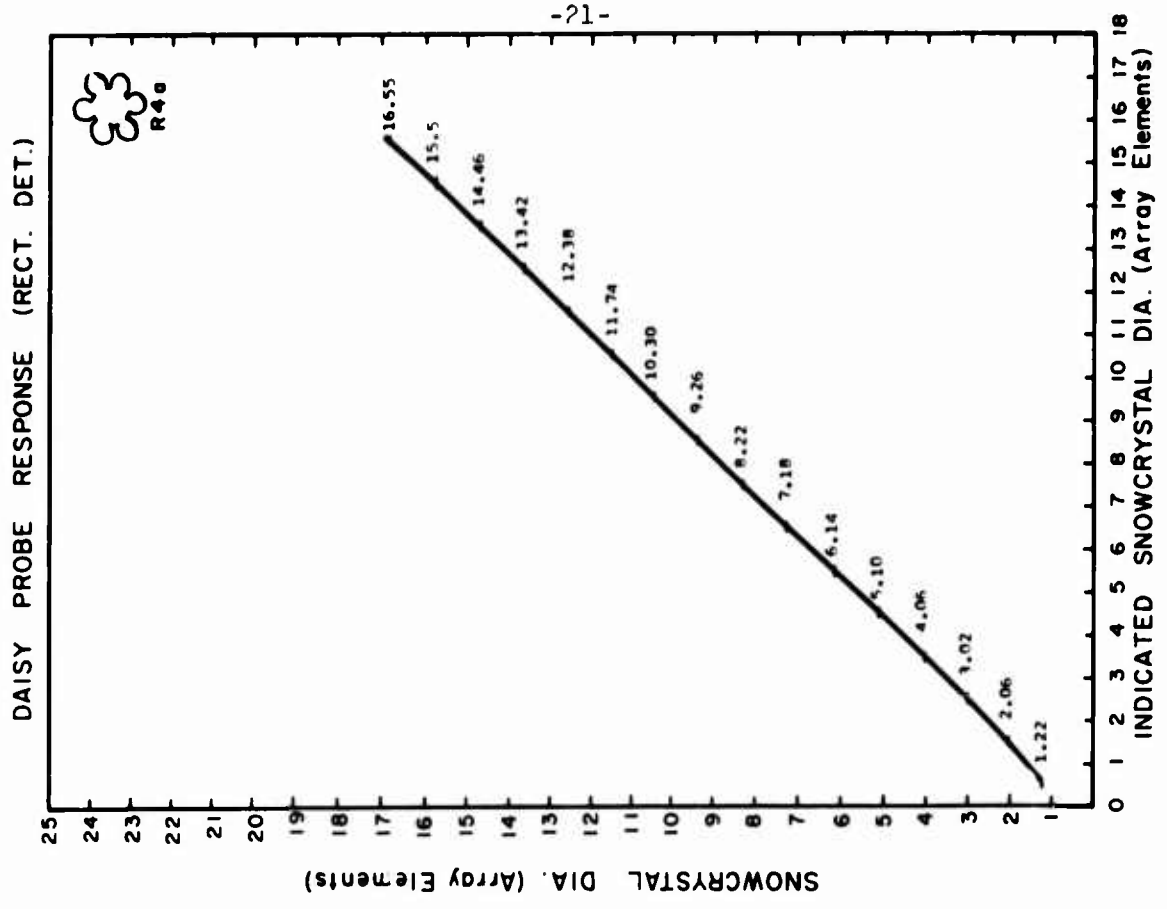

FIGURE 20

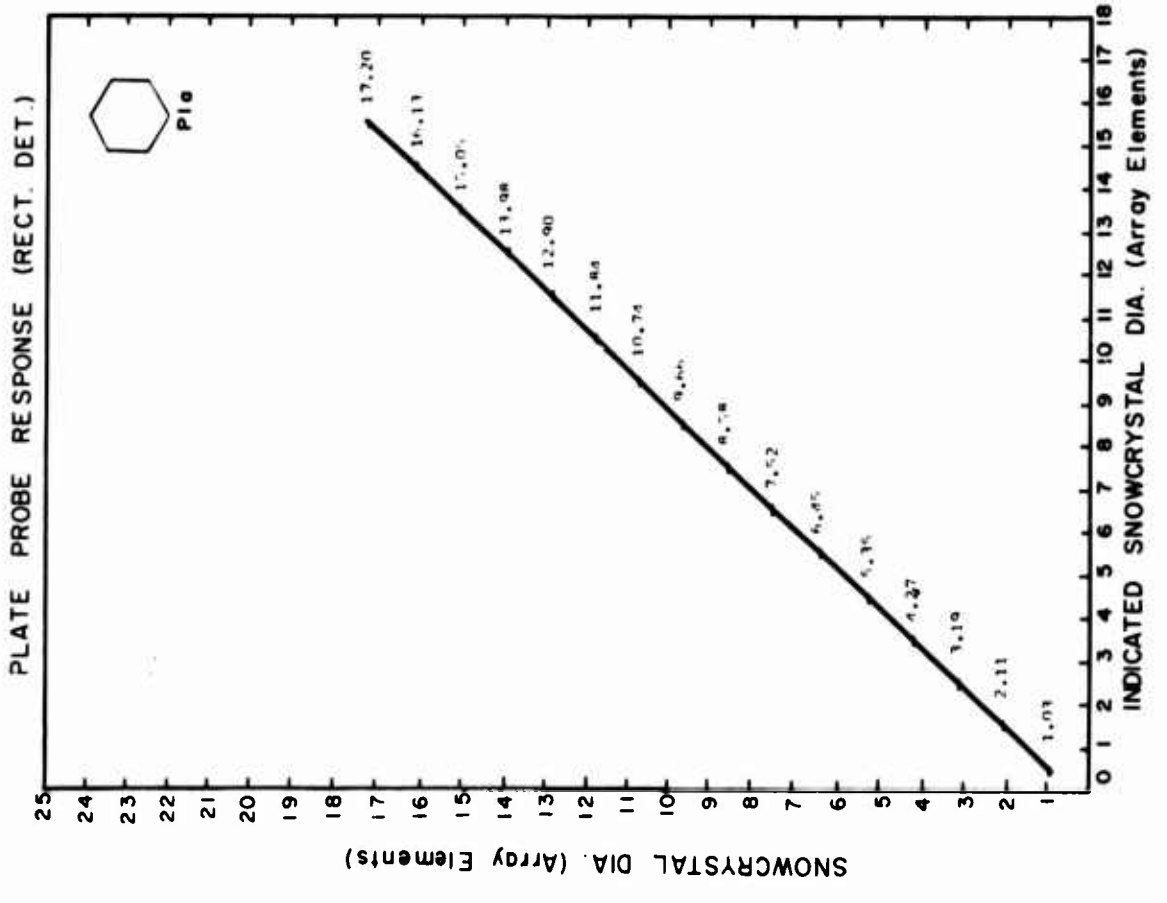

FIGURE 19

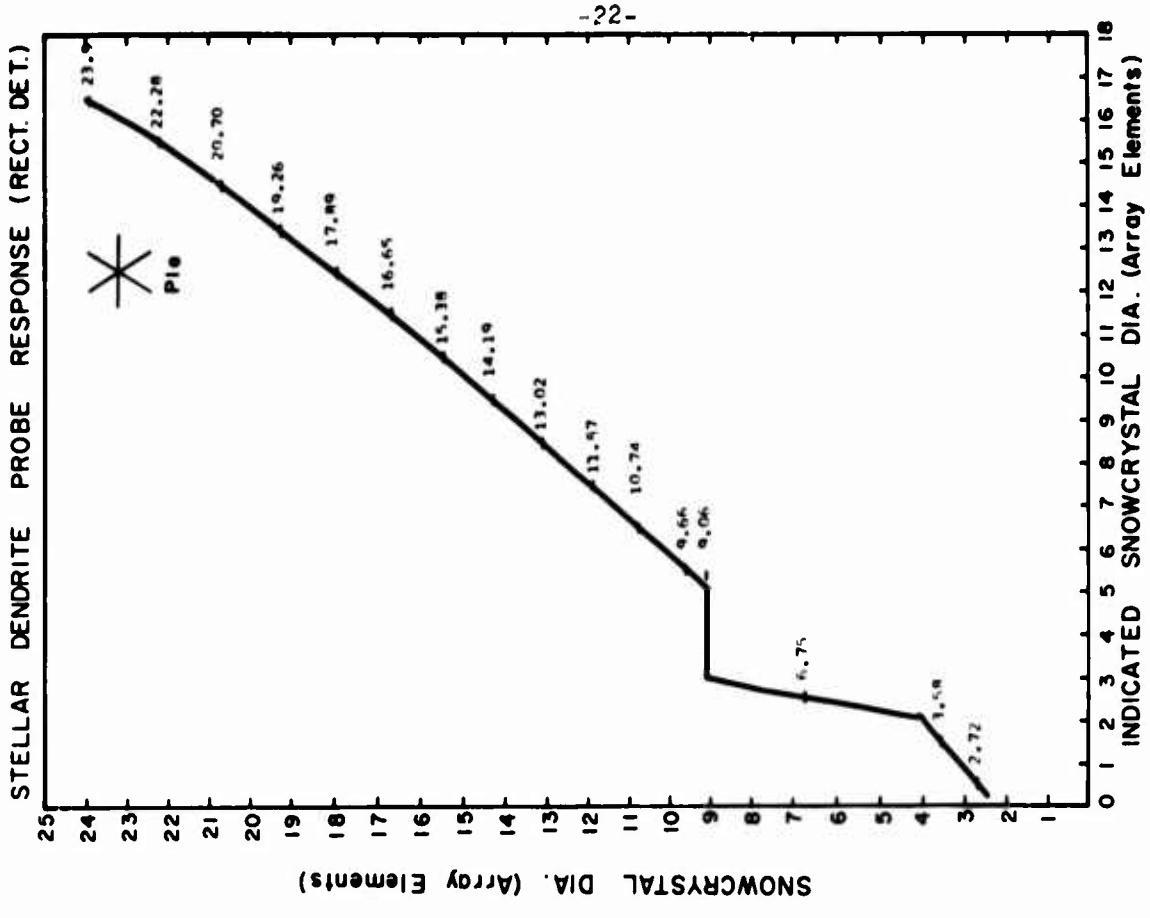

FIGURE 22

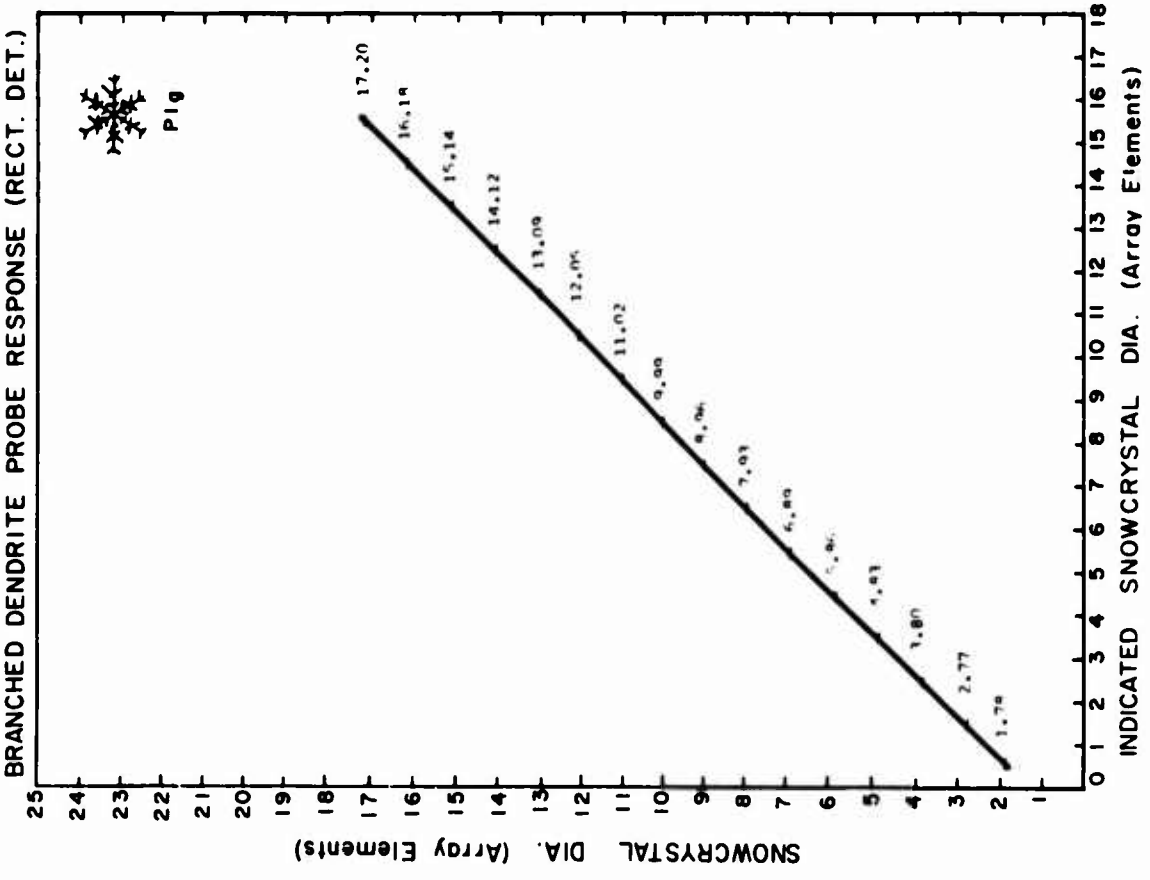

FIGURE 21

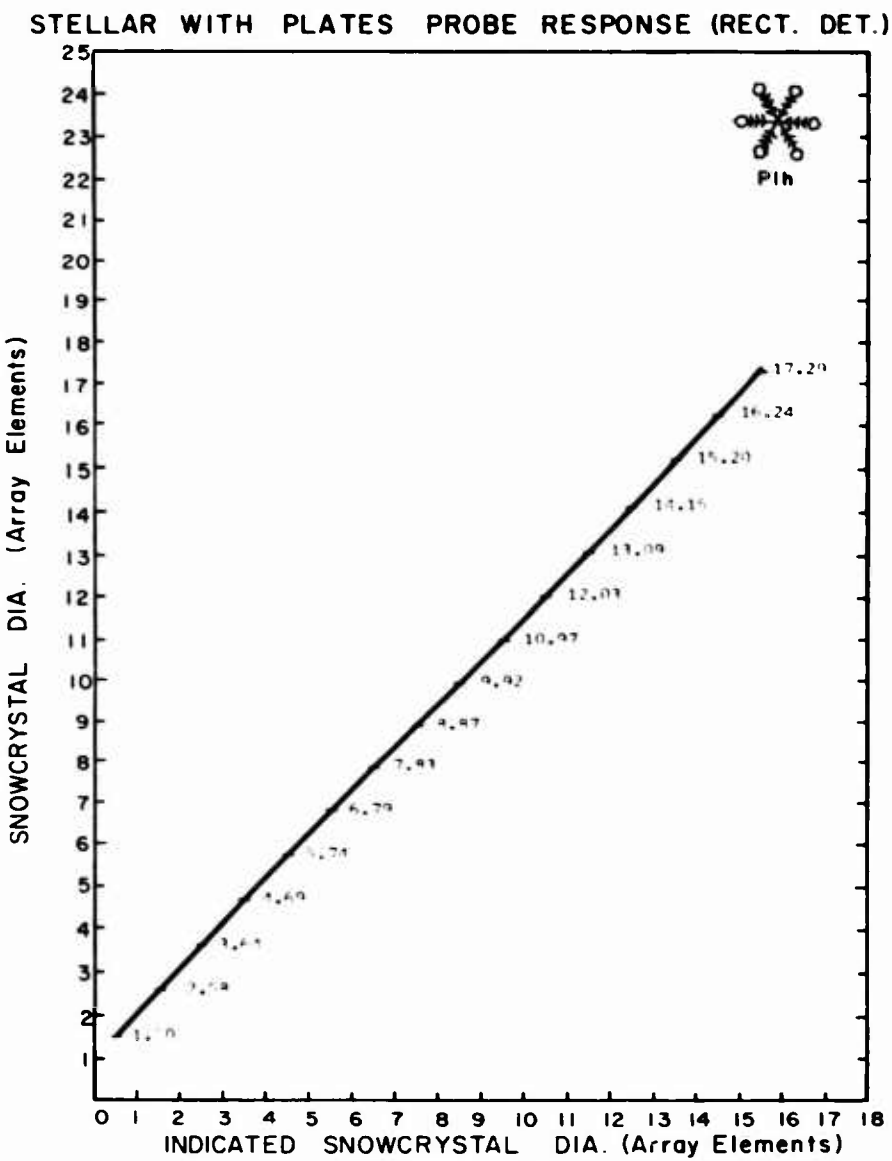

FIGURE 23

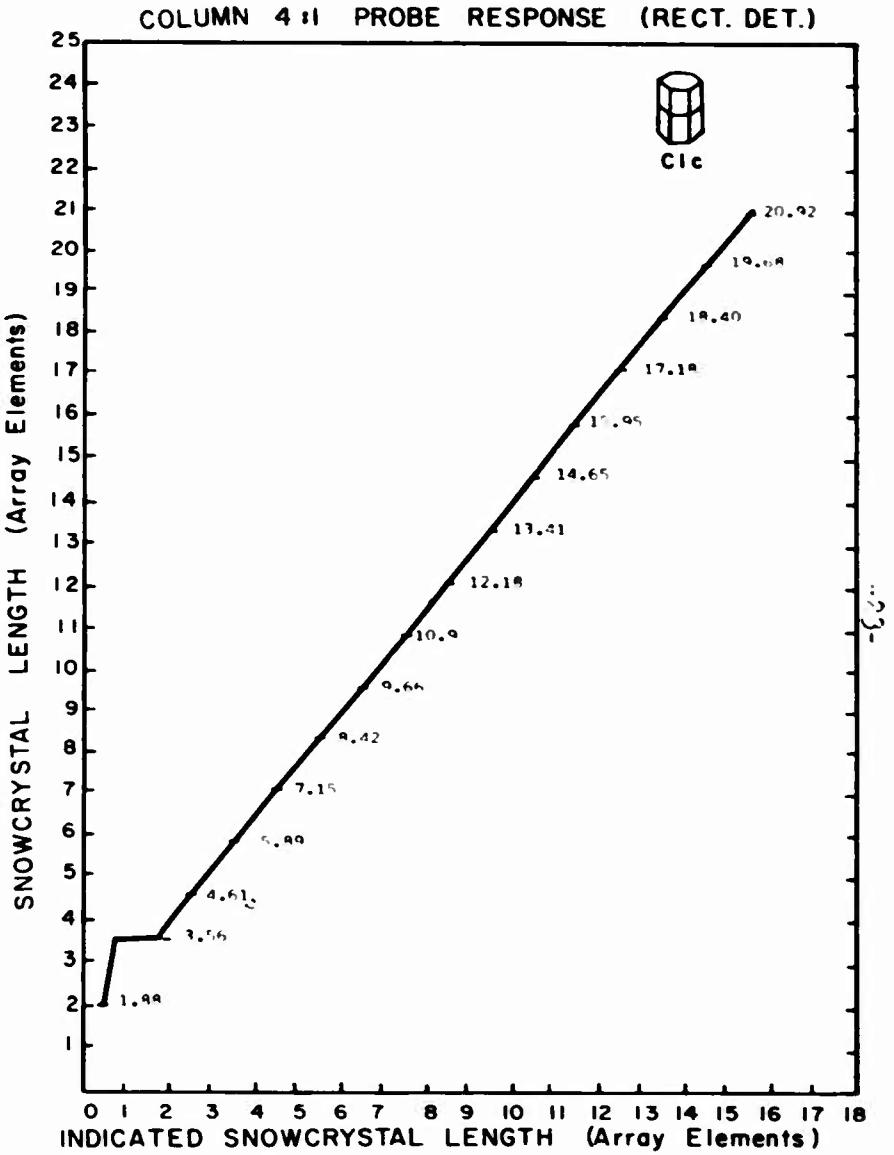

FIGURE 24

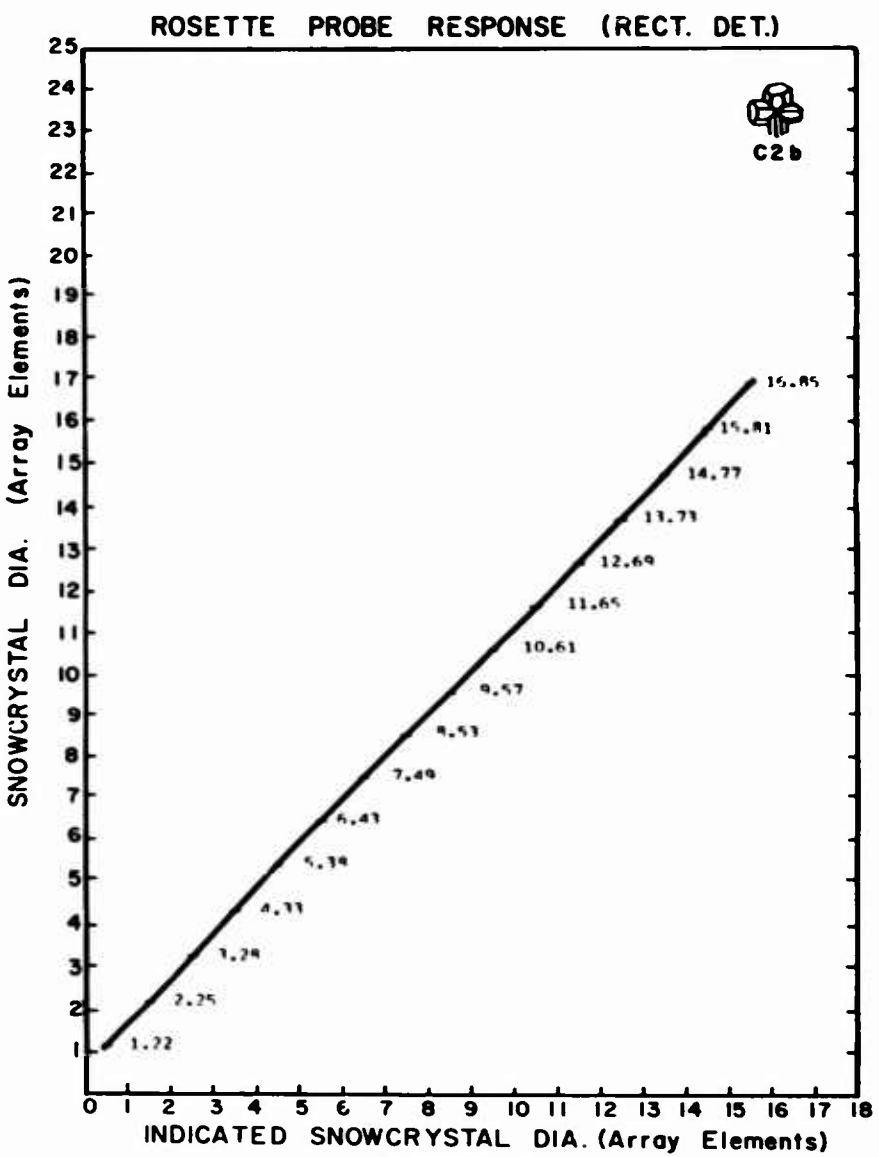

FIGURE 25

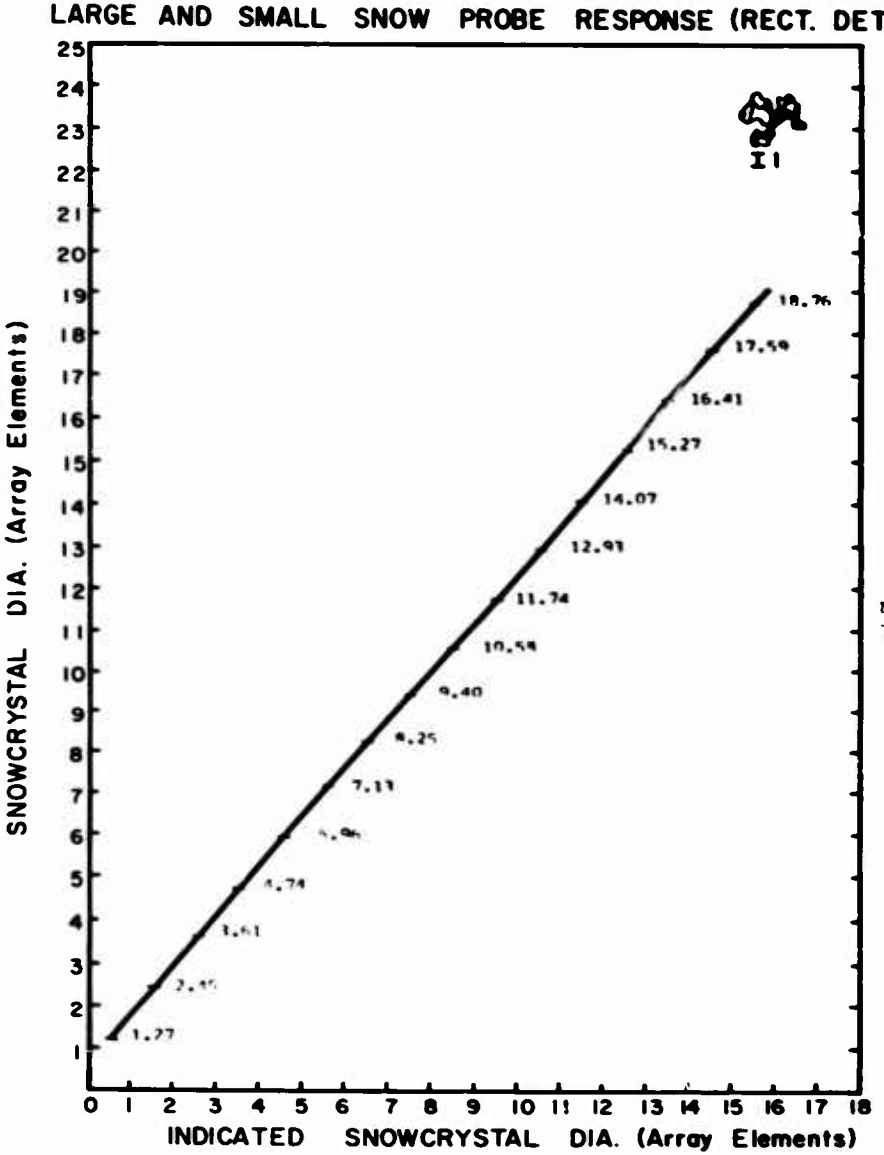

FIGURE 26

class 1 has a 25% correction factor. The disparity is greater the more complicated the crystalline habit as well as for array element shape other than spherical; i.e. the rectangular detector shown in Figure 1. A discontinuity also results in the case of the stellar dendrite of Figures 12 and 22. This discontinuity is coincident with a size where the width of a single branch covers 50% of an array element.

There are two crystalline types that are shown for the round detector geometry that are not given for the rectangular detector geometry. These are the sector plate and needle (7.5:1 aspect ratio) response functions. In the case of the sector plate, it is indistinguishable from the daisy response in Figure 20. The needles rarely register, because the needle, as defined, has to be nearly seven or eight elements in length before it is first seen. This is further complicated by the severe orientation sensitivity. An OAP with rectangular elements is essentially non-responsive to needles.

All of the response functions were computed assuming that the shadows are completely dark (in focus). It is obvious to address the question as to what happens when the image is out-of-focus. As it turns out, this is not as an important a factor as first may seem. When the shadow is out-of-focus, it is less dark, but also larger. In fact, the integrated loss over the out of focus image is identically the same until beyond the far-field. The depth-of-field limits and depth-of-field cutoff in the 200X Cloud Droplet Probe are all defined within the far-field limits. The 50% sizing threshold used in the OAP instruments insures that shadow densities are at least 50% dark. At the 50% dark level their total shadow area is

roughly twice as large as at true focus. Hence, approximately the same light level loss results. It can be shown that the error in sizing that results from the spreading in the shadow is no greater than one element if the 50% sizing threshold is maintained. In the Cloud Droplet probe (200X), a secondary threshold of 62½% must be reached by one of the occulted elements. The error is even smaller in this case. Table 2 shows the results of actual size measurements over the depth-of-field as are accomplished during routine calibration of a 200X probe. In the case of the 200Y Precipitation Probe, the depth-of-field is always truncated by the mechanical aperture for sizes 320 microns diameter and larger. The number of shadowed elements is very nearly the same as at true focus throughout the depth-of-field.

The only remaining question has to do with light transmission through pristine snow crystal surfaces. This is discussed in detail in Section 3. For the present purposes, it can be said that the on axis transmission of light through crystals does not appreciably reduce depth-of-field. In fact, the theoretical depth-of-field for long cylinders (which closely approximates many crystal features) is much greater than for an equivalent cross section in spherical form.

OAP 200X CLOUD DROPLET PROBE CALIBRATION

		Glass Bead Test Particle Sizes			
Channel	Size (u)	25 - 35u	45 - 75u	75 - 105u	210 - 250u
1	20	128	2	0	0
2	40	36	40	2	0
3	60	1	321	10	0
4	80	0	77	155	0
5	100	0	2	170	0
6	120	0	0	22	0
7	140	0	0	2	0
8	160	0	0	0	0
9	180	0	0	0	0
10	200	0	0	0	21
11	220	0	0	0	156
12	240	0	0	0	170
13	260	0	0	0	17
14	280	0	0	0	0
15	300	0	0	0	0

TABLE 2

3.0 LABORATORY INVESTIGATIONS

The results of the theoretical response studies were tested under laboratory conditions. Small crystal replicas were fabricated and statically and dynamically tested. The static testing provided a test for crystal orientation which is more difficult to control in dynamic tests. The dynamic testing was conducted to simulate aircraft velocity. Of prime importance here was the 2-D probe which allowed determination of the orientation in the dynamic tests. The importance of the 2-D probe in these tests lies in the fact that the 1-D probe response can be entirely predicted from the 2-D probe response. This, coupled with the higher resolution of the 2-D probe, made it the prime test instrument. In addition to the tests with crystal models we examined in detail the properties of snow crystal surfaces in the laboratory. This work was undertaken to examine the effects of various threshold settings with regard to the transmission properties of snow crystals. Finally, we determined the effect of various depth-of-field threshold settings on the real sample area of the OAP-200X Cloud Droplet probe.

3.1 STUDIES OF THE OAP RESPONSE TO CRYSTAL MODELS

The results of these laboratory studies demonstrated that the OAP responds to various shaped particles in a predictable manner. The 2-D probe was used exclusively during these tests. The crystal models were fabricated of plastic, metal, and silicon rubber materials (see Figure 27). The plastic materials could be machined to sizes as small as a millimeter (hexagonal rods) diameter and two to three hundred microns thick. Metal was restricted to the fabrication of small needles or columnar models. These had minor axis dimensions as small as 25u (one mil). The silicon rubber

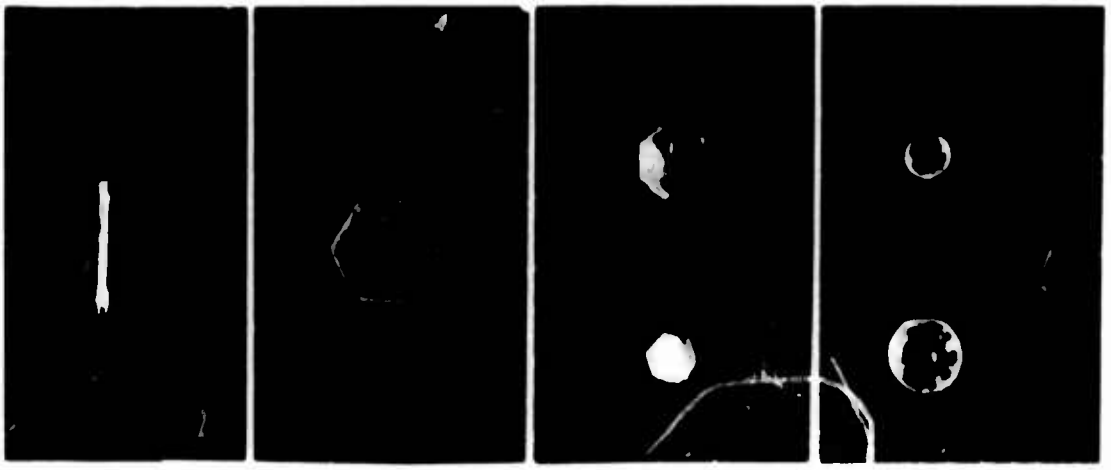

Metal Cylinder Lucite Plate RTV Plates Glass Beads

1mm

Crystal Models used for Laboratory Studies

FIGURE 27

Calibration Apparatus used for Spinning
Crystal Models through 2-D Probe

FIGURE 28

models were fabricated by casting hexagonal columns. Socket head key wrenchs were used as models in constructing the mold. The molded materials were subsequently sliced into thin (20 - 50u) plates using a microtome.[1] The silicone rubber had mass and optical properties similar to natural snow; however, the surfaces of the thin hex plates were not polished and were translucent rather than transparent in appearance.

The crystal models were tested using the calibration apparatus developed for the 2-D probe shown in Figure 28. The models were suspended by a small wire to the flywheel of the calibration device and accelerated to high velocities through the instrument field-of-view. Orientation could be changed by rotating the suspending wire. The velocity could be varied continually over a 30m sec^{-1} range. It is important to recognize that the 2-D probe allows testing in this manner whereas the 1-D probes generally would not. The 1-D probes have end element rejection mechanisms which would be triggered by the suspension wire.

The results of testing in the above manner quickly verified that the 2-D probe responded predictably to various shapes of particles. From the 2-D response the corresponding response of 1-D probes was also verified. The only differences between 1-D and 2-D response lie in the higher resolution of the 2-D probes. In general, the lower the resolution (here resolution can be thought of in terms of the number of elements occulted; high resolution thus corresponds to a large size channel event in a 1-D probe) the greater the chance of undersizing. This is, in effect, a roundoff error that increases with

---

1. A microtome is an instrument used in medical labs for slicing biological specimans into thin sections for microscope examination.

decreasing relative particle size.

On the basis of this study we concluded that it would be unnecessary to measure the probe response to each individual crystal as was proposed for the field measurements of Section 4. However, it was also apparent from the theoretical studies that the roundoff error could be quite large for certain crystal habits.

3.2 MEASUREMENTS OF THE TRANSMISSION PROPERTIES OF ICE

During the course of this work we began to receive a great deal of 2-D imagery from systems recently placed in the field. We examined several thousand particles taken with the University of Wyoming aircraft and found no evidence of disorientation of pristine crystals. There was also little indication that rimed crystal structures are disorientated although it was more difficult to verify from shape analysis. The pristine crystals, however, did show light transmission through planar faces. This was not often observed in 2-D crystal data obtained from the P3V or the C-130. In general, we attributed this to the non-rimed powder snow characteristic of the rocky mountain region. An initial examination of the possible transmission characteristics of ice indicated that there may be a real problem here. The transmission through a perfect ice crystal plane was by all estimates greater than 90%. A 50% threshold would appear to be unsatisfactory. However, the field data from the 2-D systems always indicated that the edges of all crystals are seen and that it was actually quite rare that internal transmission washed out the interior image (see Figure 29).

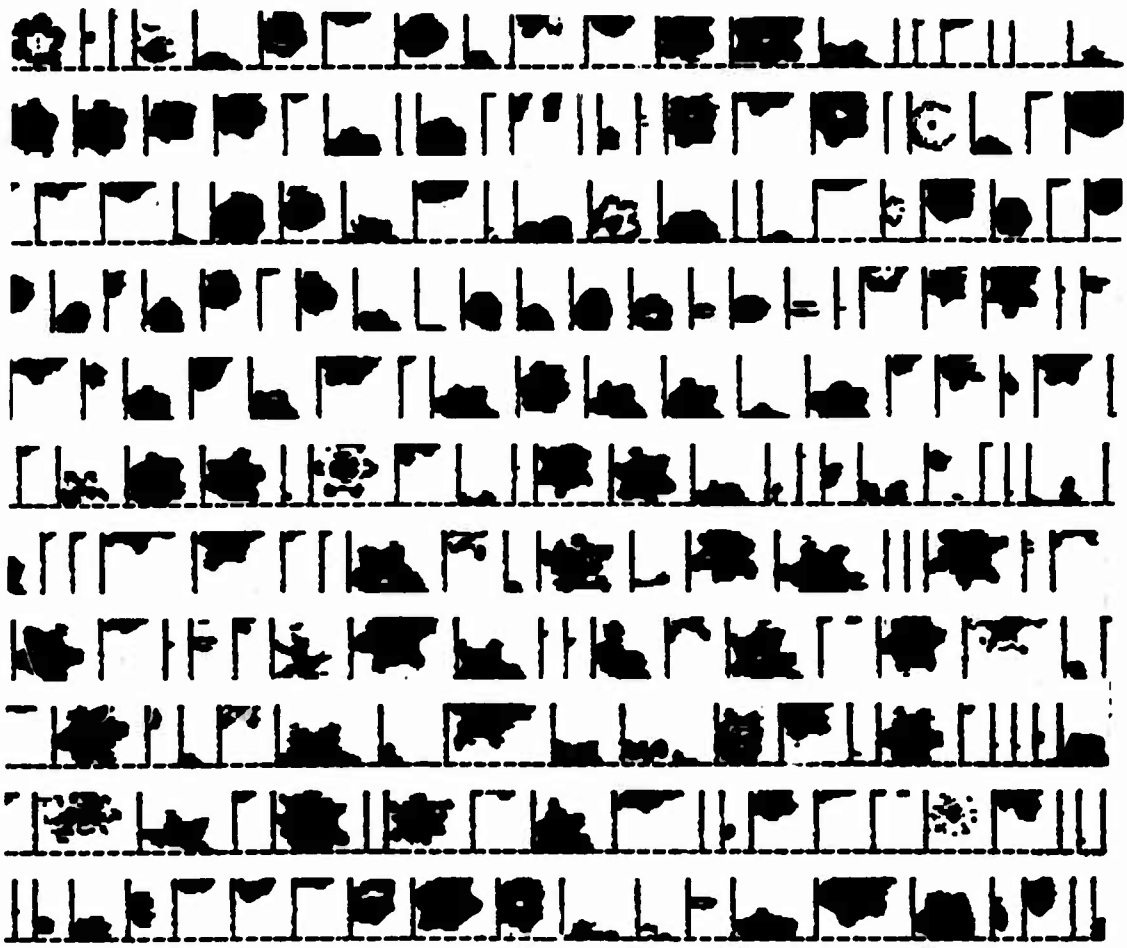

2-D Data Samples in Pristine Snow Crystals

The above samples of 2-D snow crystal data were taken by the University of Wyoming in clouds having pristine crystalline forms. Note the various crystals with various regions washed out (less than 50% occultation); however, note the general tendency for the edges of crystals to appear dark. A detailed examination revealed approximately 90% of the area of these crystals resulted in 50% or greater occultation.

FIGURE 29

Because of the large difference between the 90% transmission and the 50% threshold values we performed measurements on the reflectivity of ice at 6328A° using glass smooth ice surfaces, a He-Ne laser and a photometer. The absorption internally could be logically neglected. Measurements at 10° and 20° incident angles gave reflectivities of 2.5% and 2.9% respectively. The combined reflected loss for a single pass of a laser beam is thus between 5 and 10%. The 10° and 20° incident angles were chosen as average conditions for crystals. At 0° incident angle the value is essentially the same as that for 10°.

The reflectivity of ice was also calculated from data in the Handbook of Chemistry & Physics for the refractive index of ice versus wavelength. Data for two different refractive indices were given. These are plotted in Figure 30 and the range of refractive index for 6328A° was obtained from that graph (1.307 - 1.309). The reflectance was then calculated using Snell's law ($m \sin \phi = m \sin \phi'$) and the formula

$$R = \left(\frac{m \cos \phi' - \cos \phi}{m \cos \phi' + \cos \phi}\right)^2 \times 100\ (\%).$$

The refractive index for normal incident radiation @ 6328A° was 1.77% for 1.307 R.I. and 1.79% for 1.309 R.I. At 15° incidence the reflectance increased to 1.98% at 30° to 2.7% and at 40° incidence to 3.8%.

It would thus appear that the transmission of light through pristine ice crystals is, in general, greatly suppressed by surface and interior scattering or prismatic relief since it is rarely observed and one might suspect it to be much more

REFRACTIVE INDEX OF ICE VS WAVELENGTH

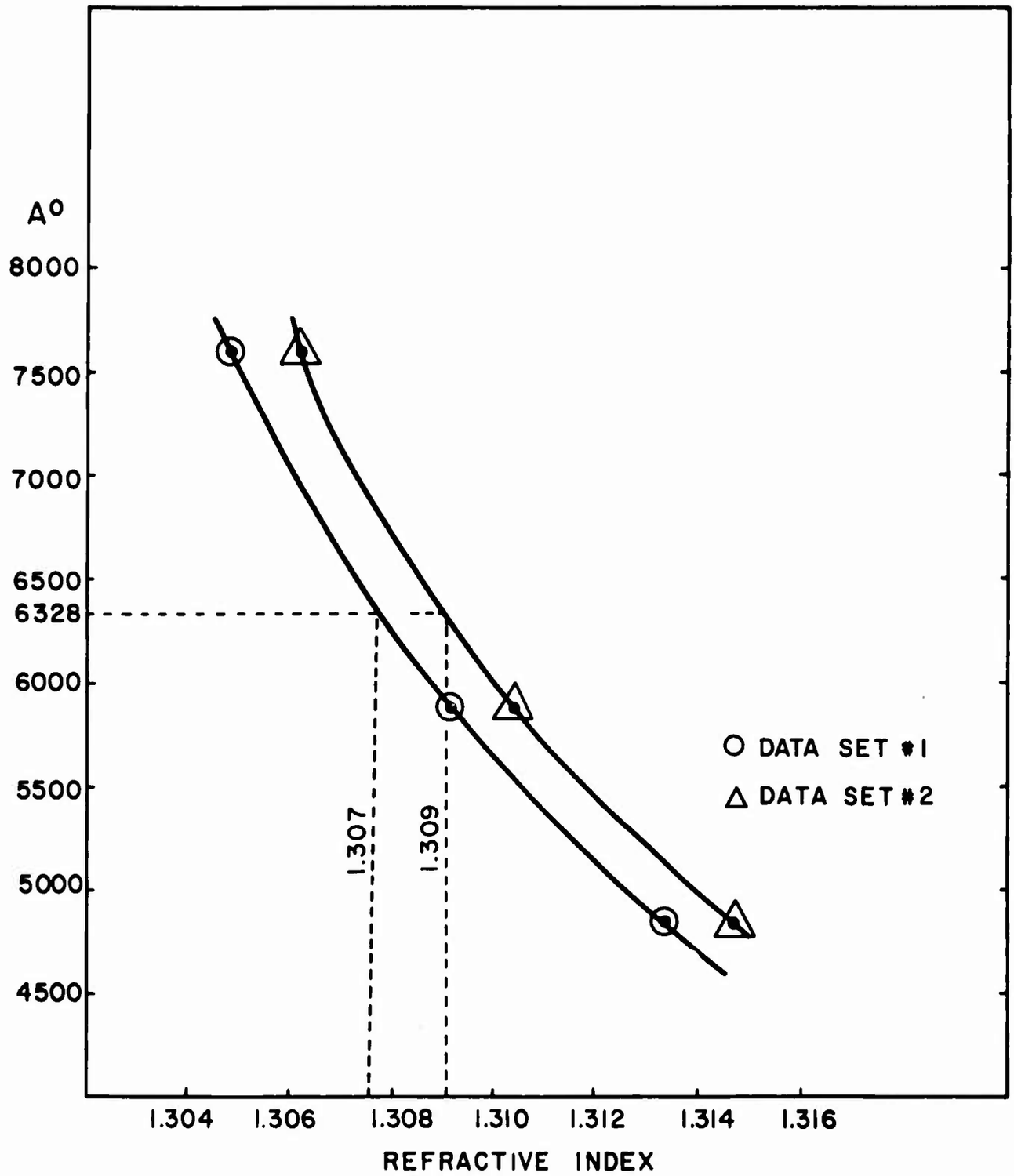

FIGURE 30

common. It is also a well known fact that the surfaces of crystals are stepped. These steps constitute a diffraction grating with predictable losses greater than 50%. Furthermore, the interior of snow crystals is sometimes translucent due to voids. All of the effects reduce light transmission; however, riming is probably the single most important factor in reducing light transmission for general snow situations of the type most often encountered by the C-130 operations.

3.3 LABORATORY SAMPLING AREA MEASUREMENTS

The accurate measurement of particle size is an intrinsic property of the Optical Array Spectrometer technique. The Optical Array Spectrometer, employing essentially a linear optical measurement technique, is also insensitive to particle refractive index, shape, color, etc. By design, the Optical Array Spectrometer will size particles accurately over it's sample volume with RMS errors not larger than the system quantitization error ($\pm$10%).

The Optical Array Spectrometer, while essentially excellent for size determination, requires very careful sampling area calibration. In all Optical Array Spectrometer instruments, the sample area is a function of particle size. Two effects are operating on the sampling area simultaneously. First of all, the depth-of-field (equal to $\pm 3.0\ r^2$) increases sample area length rapidly for increasing particle size. At the same time, the end element reject mechanism decreases the sample area width linearly with increasing particle size. The combined effect results in a sample area which at first increases rapidly with particle size and then decreases. The nominal (empirical-theoretical) value for the depth-of-field, effective array width, and the sample area are given in each OAP manual.

For the OAP-200Y precipitation probe, the depth-of-field is, in general, truncated by the mechanical probe aperture. However, the depth-of-field of the OAP-200X cloud droplet probe has secondary threshold detection to establish depth-of-field limits. In this probe, the depth-of-field and the sample area are centered about the object plane of the primary objective lens.

The sampling area width is entirely controlled by the magnification setting and is not a calibratable parameter. In order that the end element rejection is ascertained, the beam can be chopped mechanically at the object plane. Depth-of-field determination and, thus, sample area measurement requires injecting glass beads through hypodermic needles at various positions of the depth-of-field and determining the total effective (net) sampling area.

The particle sampling area calibration is as important in determining OAP performance as the particle size accuracy. This is particularly true in view of the fact that the sampling area is known to be size dependent in the case of the Optical Array Spectrometer. It is further complicated by the fact that the sampling area is not a hard and fast optically defined region, but rather is defined in terms of the probability of a shadow event registry. In other words, a particle may or may not be seen depending upon its position in the sampling volume. This is particularly true of particles falling in the first two size classes, and at positions near the extremes of the depth-of-field. Thus, proper calibration requires injecting a known number of particles through the sampling area at various depth-of-field positions and determining the fraction of observed events.

In the OAP-200X size range one has sufficient control of particle trajectories to determine the sampling area for particles > 20u diameter. For particles > 20u diameter, the sampling area was mapped using an injected number of particles at various positions within the depth-of-field.

We performed measurements at PMS for glass beads with median sizes of 24, 46, 59 and 100 microns. The tests were performed at as many as 20 positions evenly spaced within the depth-of-field. These measurements were repeated for secondary threshold settings of 64%, 72% and 82% and with hysteresis resistor values of 240K and 510K ohms. The results of these measurements show a systematic reduction in net sample area with lowered secondary thresholds. Using current secondary threshold values of 64% and 510K ohms hysteresis, the values shown in Table 3 were obtained. In effect, one should, on the basis of these measurements, reduce the sample area to the real sample area values given in the last column. A further result of this study was that there is little or no effect beyond size channel 3, regardless of the particular depth-of-field threshold settings. Likewise, the effects of varying the depth-of-field threshold settings from 60-70% were within our estimated limits of measurement error. The reduction in sample area is, in fact, an effect of capture probability (sample probability) and as long as the depth-of-field threshold does not exceed 70%, the reduction is minimal.

Since these measurements were not performed at aircraft speeds, there is an underlying question as to whether bandwidth limitation might result in further reduction of the depth-of-field and, thus, sample area. This discussion will be reserved for the final section; however, there is most likely some further reduction in sample area for these first 3 size channels where quantitization effects predominate and the effects of bandwidth limitation would be noticeable.

OAP 200X Cloud Droplet Probe
(20u - 300u Range)

Size				Depth-of-Field	Array Width	Ideal Sample Area	Sample Probability	Real Sample Area
Size Channel	Radius u	Dia. u	Calibrated Size Interval-u	mm	mm	mm^2	%	mm^2
1	10	20	14.2- 34.0	1.0	.44	0.44	26%	0.11
2	20	40	34.0- 54.2	4.0	.42	1.68	62%	1.04
3	30	60	54.2- 73.6	9.0	.40	3.60	89%	3.20
4	40	80	73.6- 93.6	16.0	.38	6.08	100%	6.08
5	50	100	93.6-113.2	25.0	.36	9.00	100%	9.00
6	60	120	113.2-132.8	36.0	.34	12.24	100%	12.24
7	70	140	132.8-152.6	49.0	.32	15.68	100%	15.68
8	80	160	152.6-172.4	61.0	.30	18.30	100%	18.30
9	90	180	172.4-191.8	61*	.28	17.08	100%	17.08
10	100	200	191.8-212	61*	.26	15.86	100%	15.86
11	110	220	212 -231	61*	.24	14.64	100%	14.64
12	120	240	231 -250	61*	.22	13.42	100%	13.42
13	130	260	250 -270	61*	.20	12.20	100%	12.20
14	140	280	270 -290	61*	.18	10.98	100%	10.98
15	150	300	290 -310	61*	.16	9.76	100%	9.76

* Limited by Probe Aperture

Sample Area Parameters for OAP-200X Cloud Droplet Probe

TABLE 3

4.0 FIELD MEASUREMENTS OF SNOW CRYSTAL SIZE AND MASS

The primary method of correlating the probe-indicated snow crystal size with melted diameter originally proposed involved the measurement of single snow crystals by an Optical Array Probe, and comparing both the crystal size and melted droplet size photographed with a camera. Sampling apparatus was developed to accomplish these measurements and is described in Section 4.1 below. In the course of this study several sources of new information were obtained which made the simultaneous measurement as described unnecessary. This allowed the use of a much simpler 35mm camera with a fixed stage to simply photograph snow crystals and,after melting, re-photograph to determine melted diameter. This camera method described in Section 4.2 provided a much larger data base than could have been achieved with the more complicated OAP sampling system.

The primary factor that allowed us to preclude using the OAP sampling system approach for the bulk of our field measurements was that all available evidence showed that the OAP response to snow crystals was entirely as predicted. This evidence came from several sources. First,laboratory studies involving snow crystal models (see Section 3.2) showed that the OAP responded predictably to simulated snow crystals. Second, 2-D data began arriving from various sources wherein the imagery left no uncertainty as to the correctness of the OAP response to snow crystal dimensions.* Thirdly, early

---

* The primary source of 2-D data was from an instrument used by the University of Wyoming in pristine snow crystal environments. Data from the C-130's and a Navy P3V were also examined to determine possible probe mis-sizing. Early results indicated that some planar unrimed crystals showed transmission in the interior; however, the edges of crystals (prismatic faces) were always fully shadowed and thus the maximum size was always measured when the probe had adequate resolution. In non-pristine snow crystal environments the snow crystals invariably gave solid images.

measurements using the OAP sampling system gave results that were entirely predictable from the theoretical response functions being generated for snow crystals of various habit.

We therefore established the 35mm camera approach as our primary field tool for snow crystal melted diameter measurement. Using this method we were able to photograph nearly 3,000 snow crystal/droplet diameter pairs and deduce melted diameter relationships for fourteen snow crystal types.

4.1 THE OAP SNOW CRYSTAL SAMPLING SYSTEM

This system was designed to sample snow crystals at ground level during natural snowfall. The function of the system was to allow crystals to flow through the OAP sample volume in a manner that their maximum dimension would be sized. After a crystal passed through the instrument field-of-view (FOV) it landed on a photographic stage where it was photographed, melted, and re-photographed. The probe-measured diameter, photographed crystal size, and melted diameter were used to establish the relationship between probe-measured size and ice crystal mass. The photograph of the snow crystal prior to melting provided a check of the theoretical and laboratory determined probe response characteristics.

The airflow device designed for the system was powered by vacuum and is shown in Figure 31. The air flow from outside passes through the accelerating intake, through the FOV of the OAP and subsequently through a cloth photographic stage to the vacuum pump. A throttle was included in the intake section so that the air flow could be varied as required.

Preliminary tests were conducted with the device using simulated snow crystals. The simulated crystals were fabricated by casting hexagonal columns of translucent silicon rubber. The columns were then sliced into thin (20 - 50u) plates using a microtome. The thin hex plates had mass & optical characteristics similar to natural snow which made them useful in the initial phase of testing.

The OAP snow crystal sampling system was also tested with natural snow. Testing was almost entirely with the 2-D probe although short runs were also made with the 1-D probe

Snow Crystal Sampling System
Mounted on 2-D Probe

FIGURE 31

using a manual reset. In natural snow we were able to establish that the OAP response was as expected with few surprises. One problem not expected,however, was with crystal orientation. Tests verified that in the boundary layer near ground level snow crystals are not as well oriented as they are at flight altitudes. Our examination of several thousand snow crystals taken with the University of Wyoming aircraft found no evidence of disorientation of pristine crystals. There was also little indication that rimed crystal studies were disoriented as well. Additional problems encountered were those of determining which snow crystal passed through the field-of-view during heavier snow, snow crystal break-up on impact with the photographic stage, and water droplet size uncertainty due to the irregular surface of the porous cloth stage. By devising proper field methods and increasing operating skills these difficulties were largely overcome; however, the data collection efficiency of the camera with fixed stage could never have been approached.

We have collected approximately two hours of data during one natural snowstorm using this system. We took sporadic photographs of particles during these operations to verify certain easily recognized crystals. Most of these crystals were aggregates; however, intercomparison invariably resulted in identifiable crystals that passed through the instrument. Because over two million images exist on these tapes, data analysis was never attempted.

4.2 35mm CAMERA WITH FIXED STAGE

A 35mm camera with a fixed stage was used to photograph the snow crystals and their melted diameter. The stage was black anodized aluminum and coated with paraffin. The paraffin coating caused the water from the melted snow crystals to form nearly spherical droplets which made precise water content determination possible. The stage was positioned for 1-1 magnification. Extension tubes were required to properly locate the lens. The effect of field curvature resulting from the 1-1 magnification was reduced to an acceptable level by careful focusing and using a high f/# (f/11-f/16) when taking the photographs The camera and stage are shown in Figure 32. Plus X film was used to photograph the snow crystals and water droplets. When a snow crystal fell in the field-of-view (FOV), a photograph was taken. Another photograph was taken after the snow crystal melted and the water droplet was formed. It was possible to maintain the plate temperature slightly above freezing so that the snow crystal landed on the plate and remained frozen a few seconds before melting. This allowed time to photograph the frozen snow crystal before it melted without requiring a long wait for melting so the droplet photograph could be taken. An occasional cooling in a snow bank or warming with a hand was sufficient to control the melting time. This control was necessary because when the plate was too warm the snow crystal melted before a photograph could be taken. When too cold the snow crystals did not melt quickly enough which increased the chance of another crystal landing in the same area causing a loss of data for that event. Each snow crystal that fell in the camera FOV was photographed. This gave an accurate statistical distribution of the relative

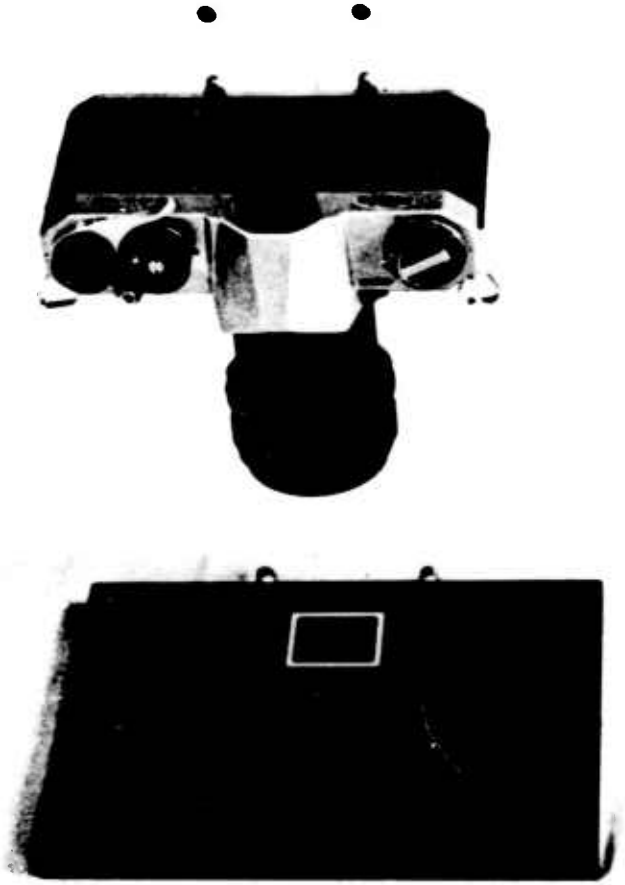

35mm Camera with Fixed Stage
Used for Field Photography of Snow Crystals

FIGURE 32

frequency of occurrence of the different snow crystal classes. An occasional "nice" crystal was assisted in landing in the camera FOV but this was kept to a minimum.

4.5 SUMMARY OF FIELD MEASUREMENTS

Field studies were carried out during natural snowfall in and around Boulder, Colorado in March, April and May, 1975. The collecting elevation varied from 5,000 to 10,000 ft. Approximately 110 rolls of film were taken; 30% of which were 20 exposure rolls and the remainder 36 exposure. This resulted in a total of 3540 frames shot during the field studies and approximately 2800 snow crystal/water droplet pairs were recorded. The events with water droplets missing or which were questionable for some reason were eliminated. All of the snow crystal data were taken during daylight hours. One attempt was made to photograph crystals at night which was unsuccessful due to inadequate light and cold temperatures.

The melted snow crystal water droplets did not form true spheres. Through measurements it was determined that the droplet height was 65% of the diameter. A calibration was established by measuring the diameter and height of droplets of various size on the paraffin coated stage. The droplet height was determined using the micrometer readout on a Unitron Microscope stage as a measuring cathetometer. The difference between reading at the top of the droplet and the surface it rested on gave the droplet height. The diameter was determined by photographing droplets at a calibrated magnification. The water droplet volume was then calculated and converted mathemetically to the equivalent sphere. The average water content for each snow crystal type was graphed showing the snow crystal diameter vs water droplet diameter.

Shown in Table 4 is a list of the crystalline types that

COLLECTED SNOW CRYSTAL TYPE DISTRIBUTION

Snow Crystal Type	Code	# Collected	% Collected
Hexagonal Plate	P1a	301	10.78
Sector Plate	P1b	85	3.04
Daisy	P1d	79	2.83
Branched Dendrite	P1c	414	14.82
Spatial Dendrite	P5a	30	1.07
Plane Dendrite	P1f	Included with Branched	
Stellar Dendrite	P1e	228	8.16
Rimed Dendrite	R3b	117	4.19
Stellar w/End Plates	P1h	92	3.29
Needle	N1	46	1.65
Column	C1c	59	2.11
Rosette	C2a	38	1.36
Small Snow	I1	1107	39.61
Large Snow	I1	185	6.62
Grauple	R4b	13	.47
Total		2794	100.00

TABLE 4

have been identified from approximately eleven weather systems from which data had been obtained. Also given is the number of crystals of each type observed. Of the 2794 total crystals 276 were rimed single crystals and there were 160 fragments. The small snow and large snow categories invariably contained rimed crystal elements. Where recognizable pristine crystals occurred within the "snow" types notation was made. It is our judgement that these snow categories contain at least 95% rimed crystalline structures. If one considers half of the snow fragments to be rimed as well the overall percentage of rimed crystals is 56.7%. We were able to develop a separate crystal type in the case of the dendrites as rimed dendrites. It should also be pointed out that most of the crystals in the large and small snow categories were aggregates of rimed dendrites. Aggregates of plates were extremely rare. The results of the field measurements and subsequent laboratory examination are presented in Figures 33-46. These fourteen figures cover a range of crystal sizes from approximately 200u to over 6mm; however, the bulk of the data is between 0.5 and 3.5mm. The curves are drawn through points representing the average melted diameter for a given crystal size. This was necessary because of the great number of data points in many cases. The standard deviation for selected data regions are given on each curve as well as the number of individual measurements represented by each data point.

In general the results of these measurements are quite similar to previous results. For some of the crystalline types no prior data exists (e.g. daisy, small and large snow, stellar etc.) for comparative purposes. There is one significant difference between our data for the branched dendritic family. These data in Figure 36 show a curve with an increasing rate of mass gain with size. There is also some evidence of this

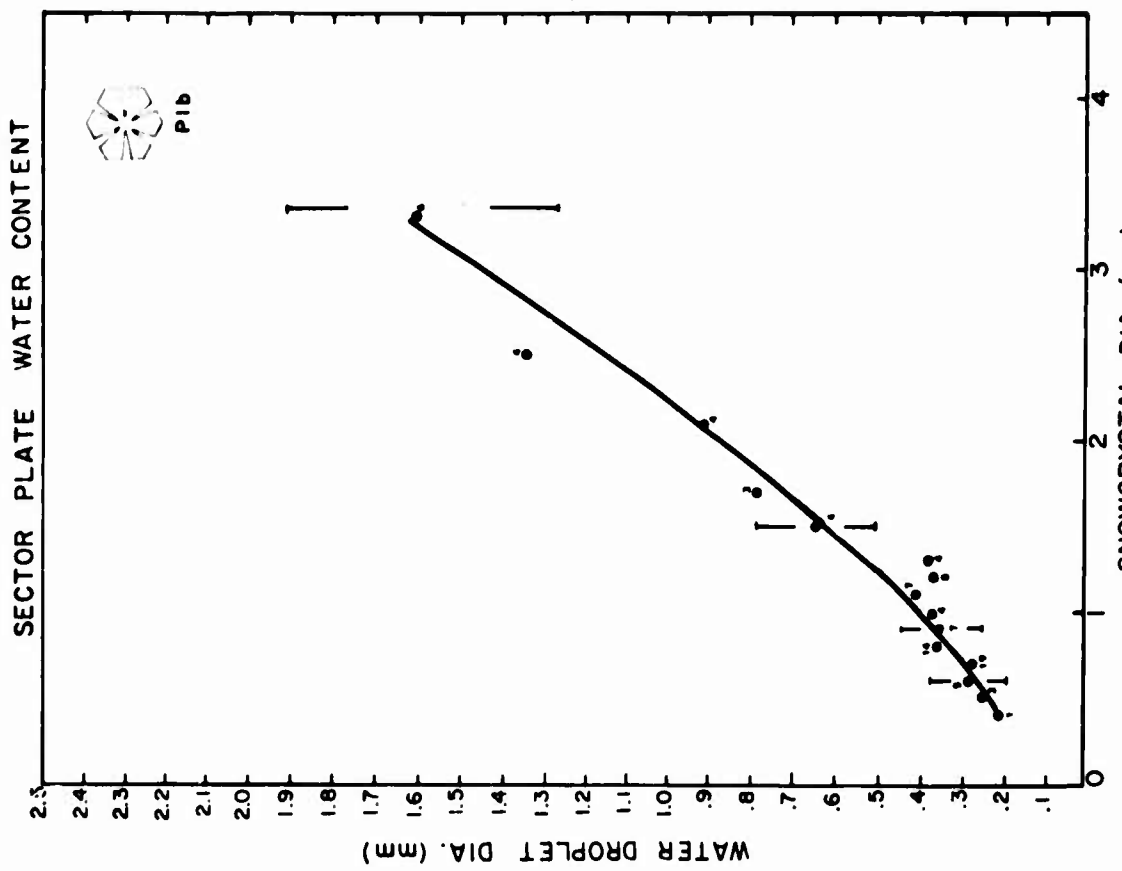

FIGURE 34

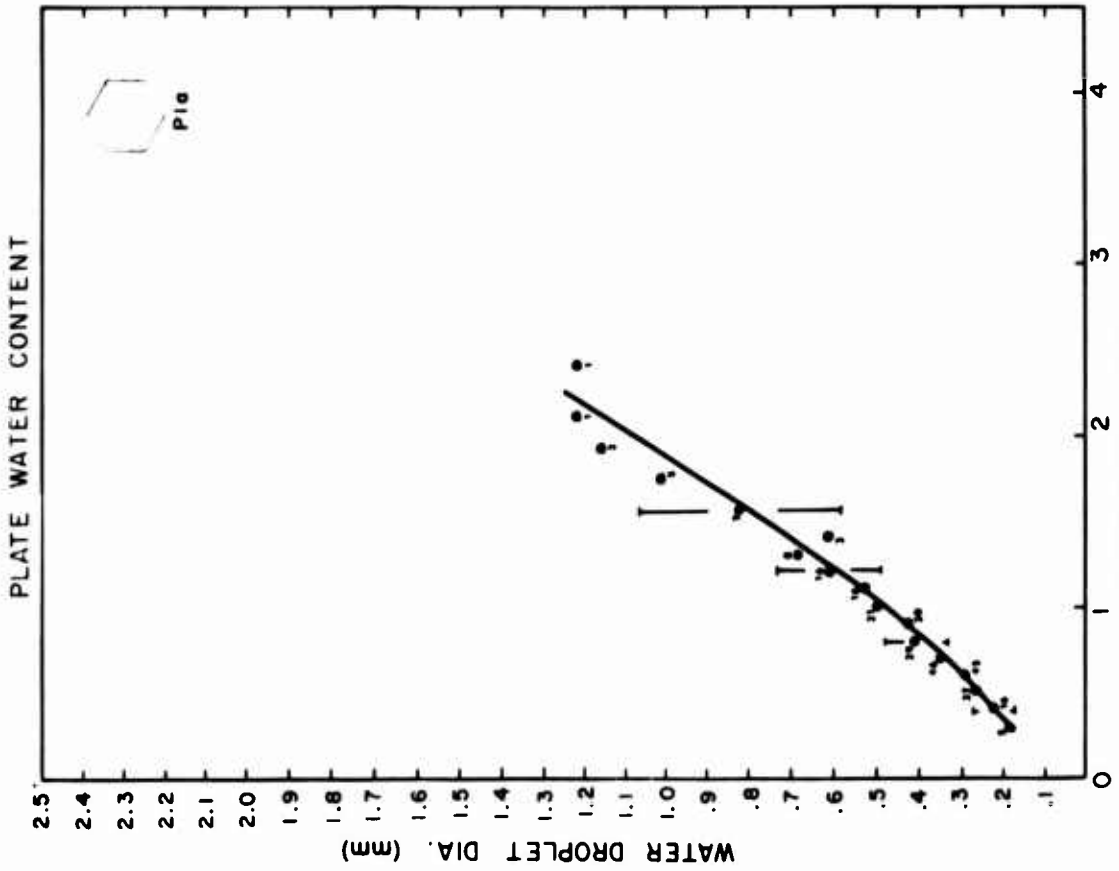

FIGURE 33

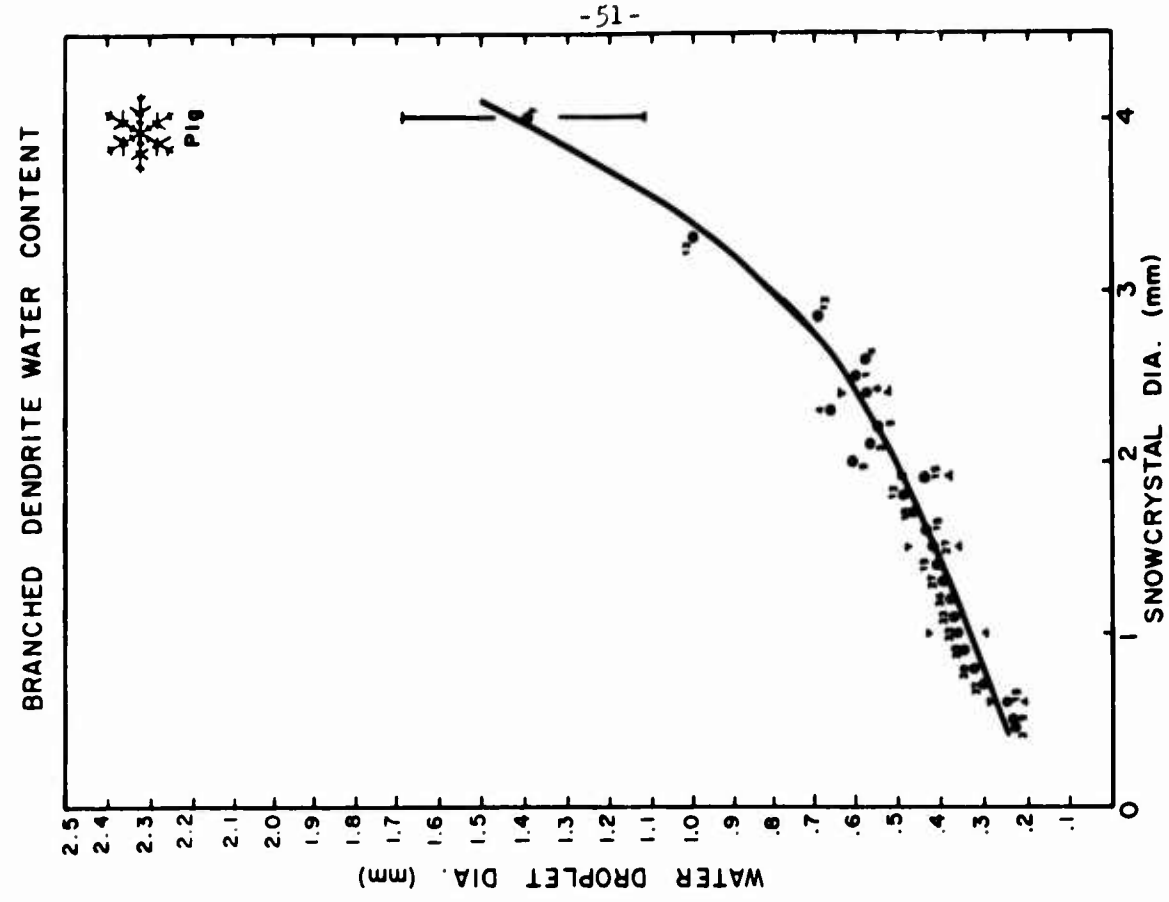

FIGURE 36

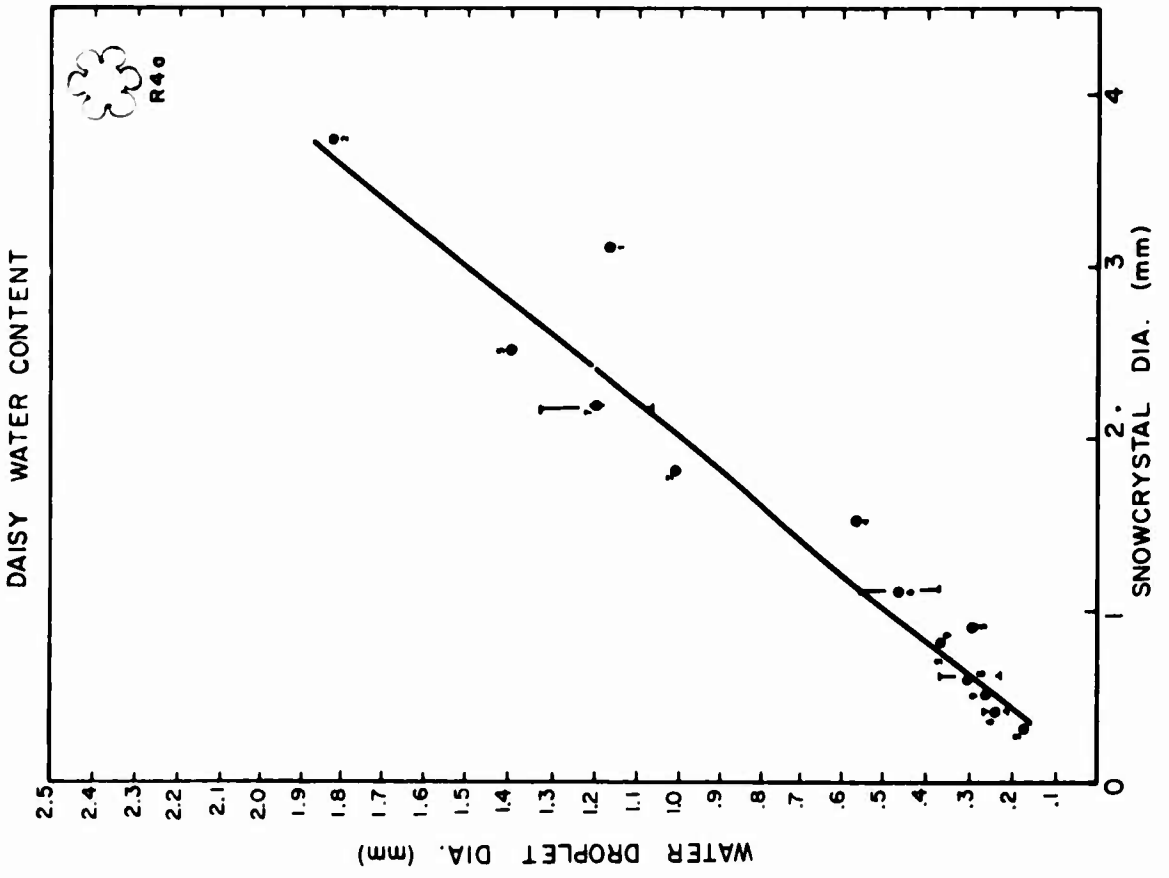

FIGURE 35

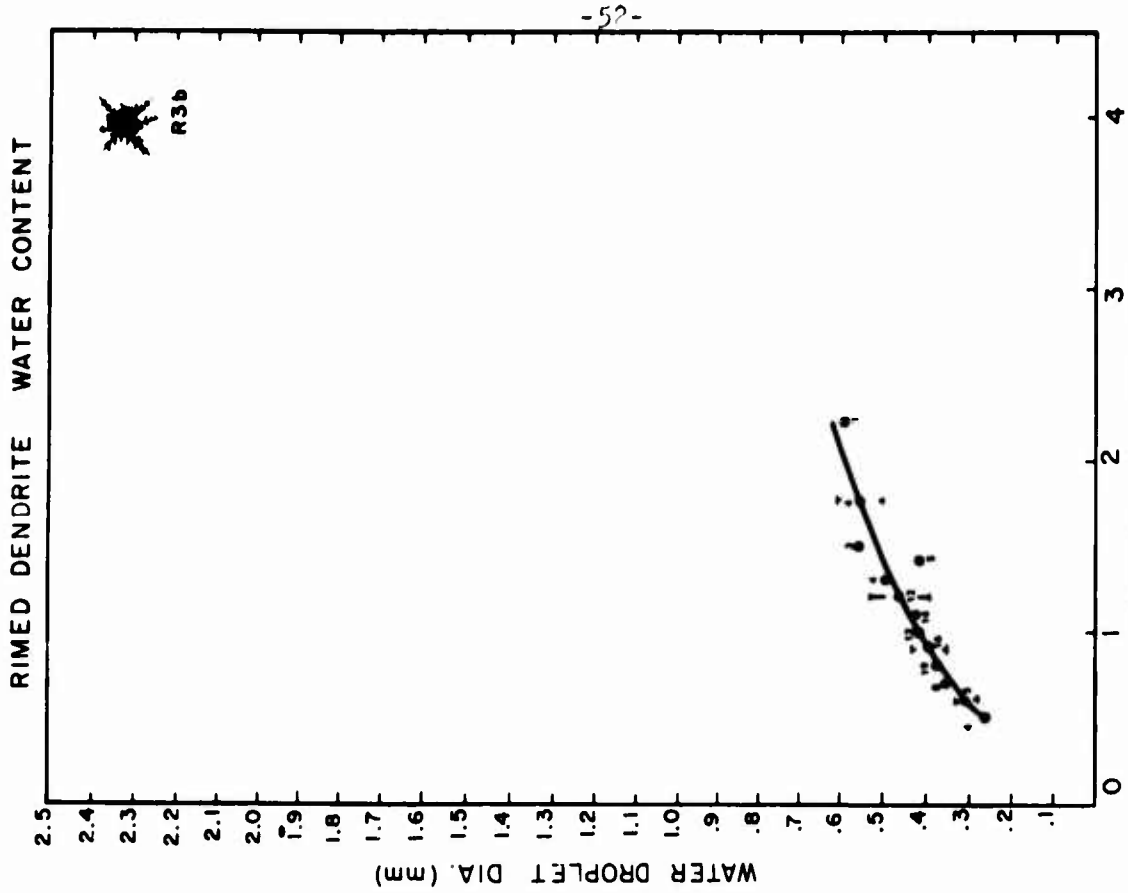

FIGURE 38

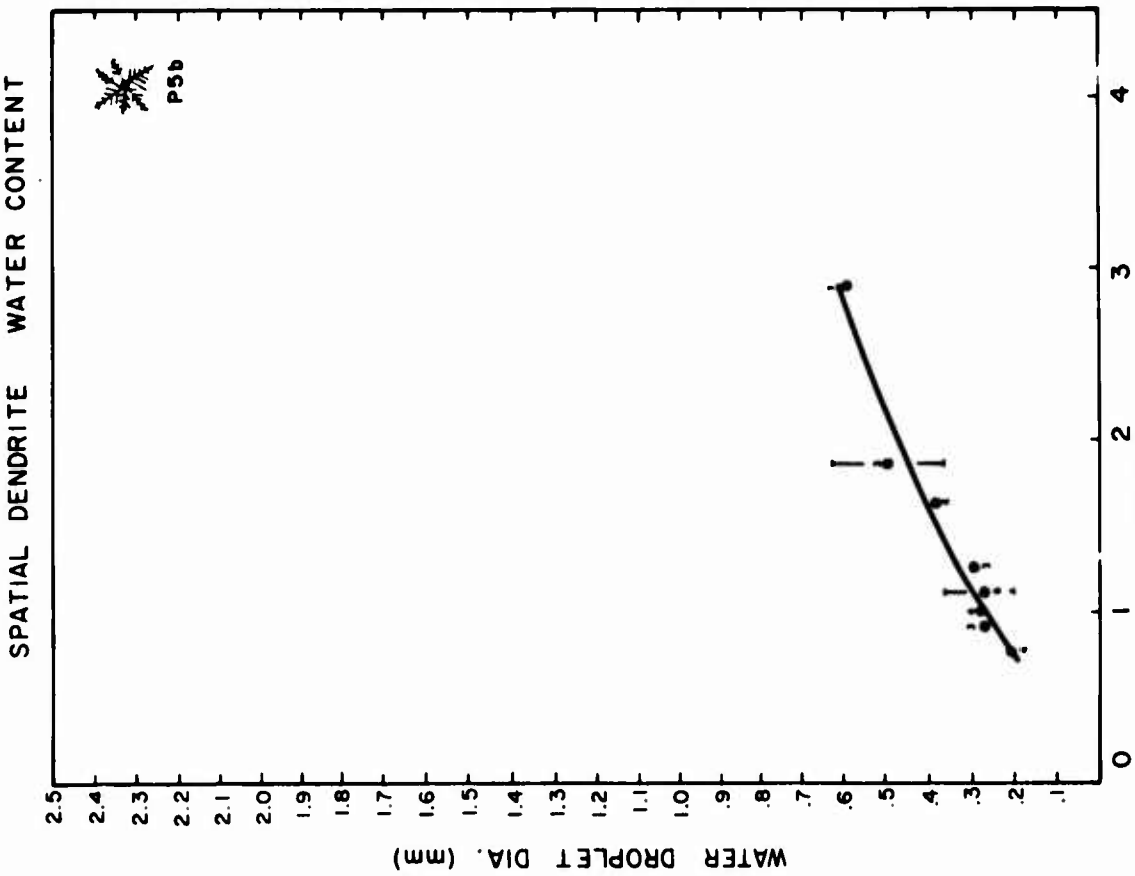

FIGURE 37

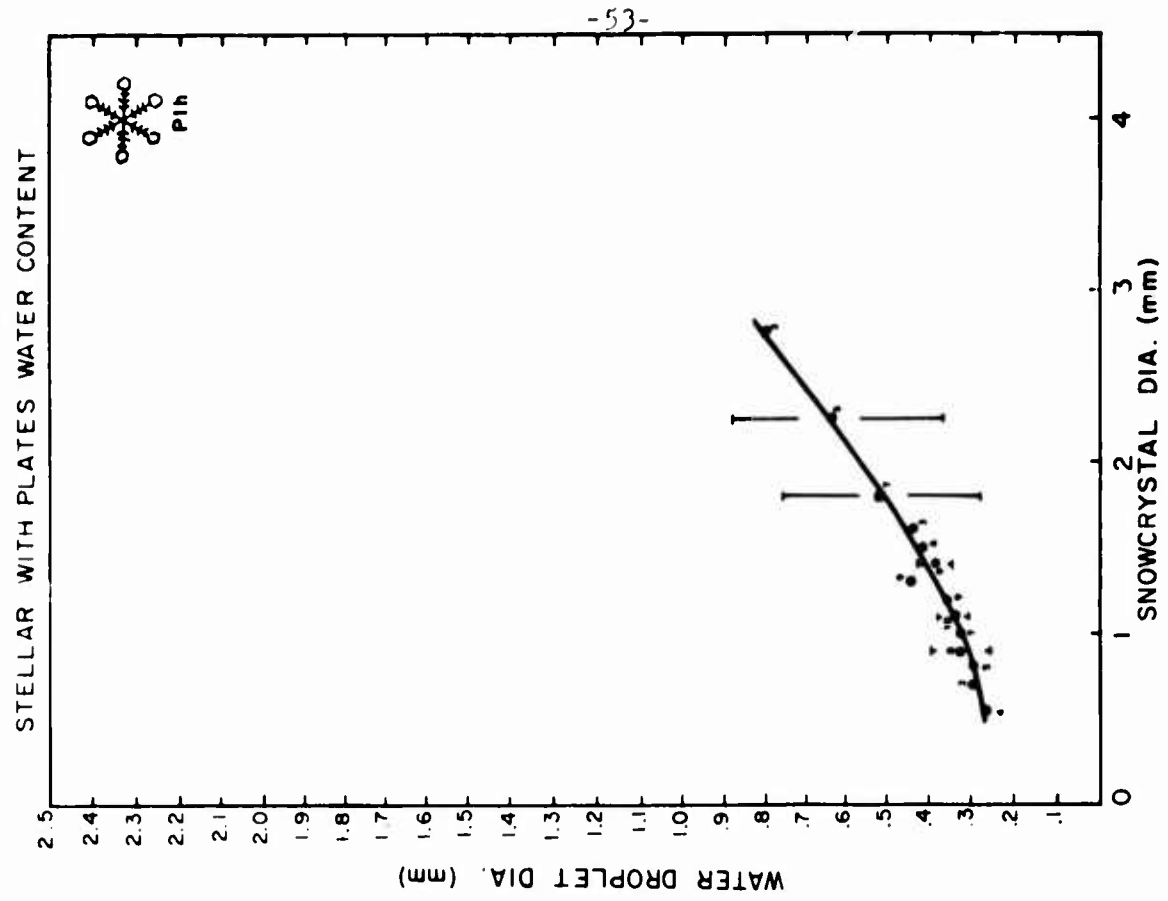

FIGURE 40

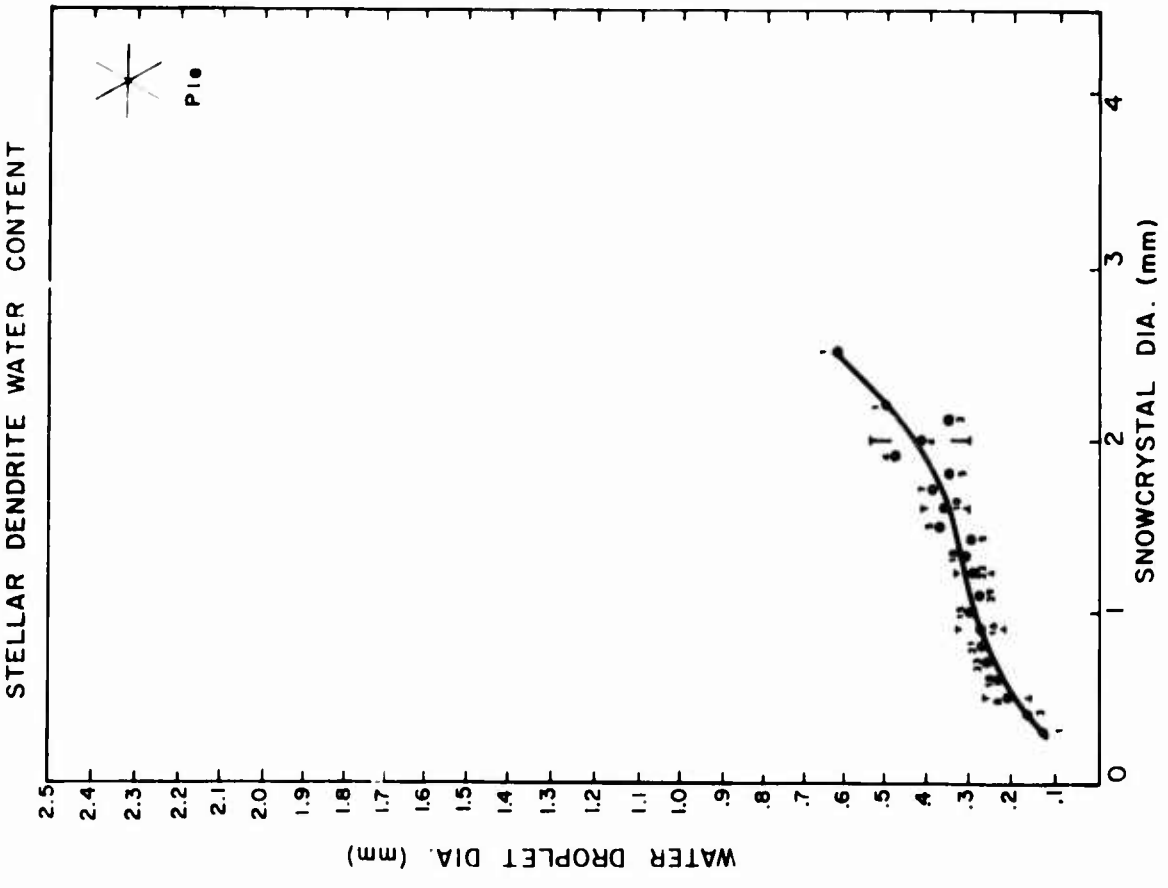

FIGURE 39

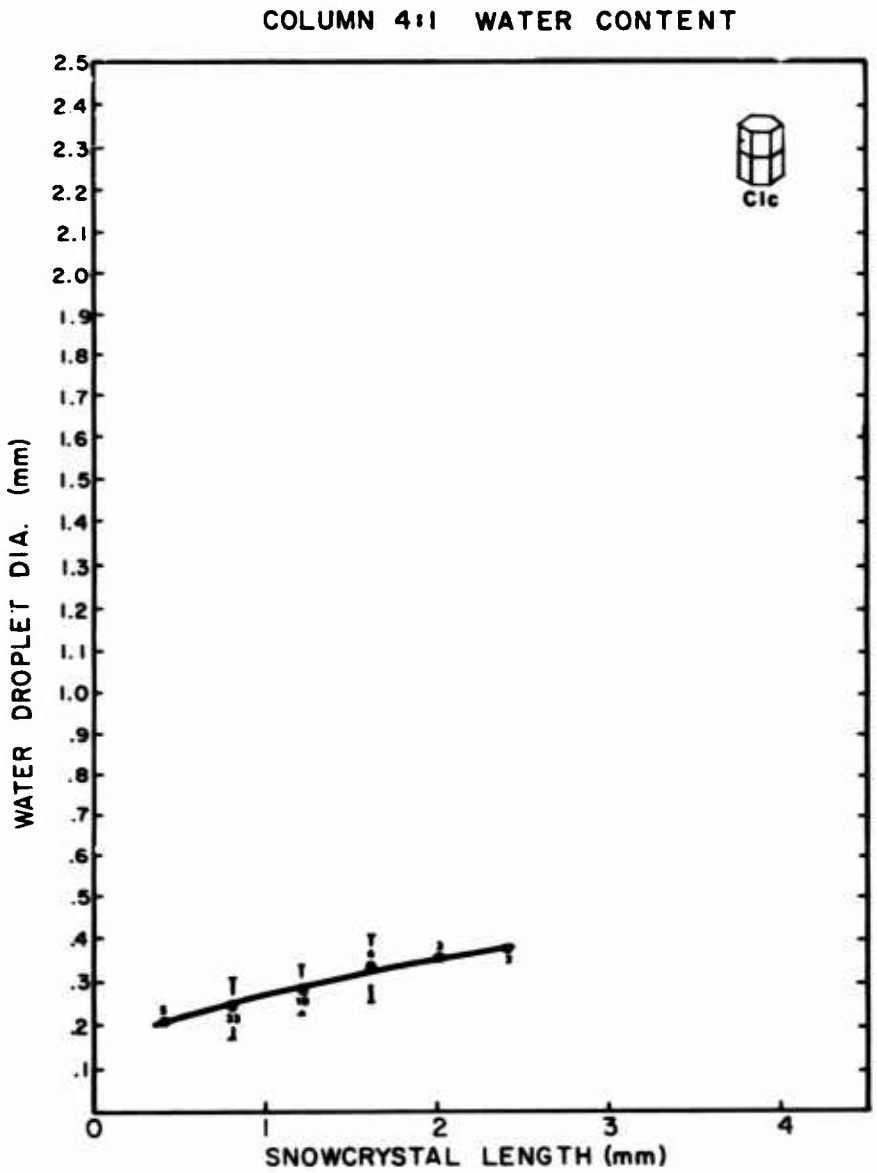

FIGURE 41

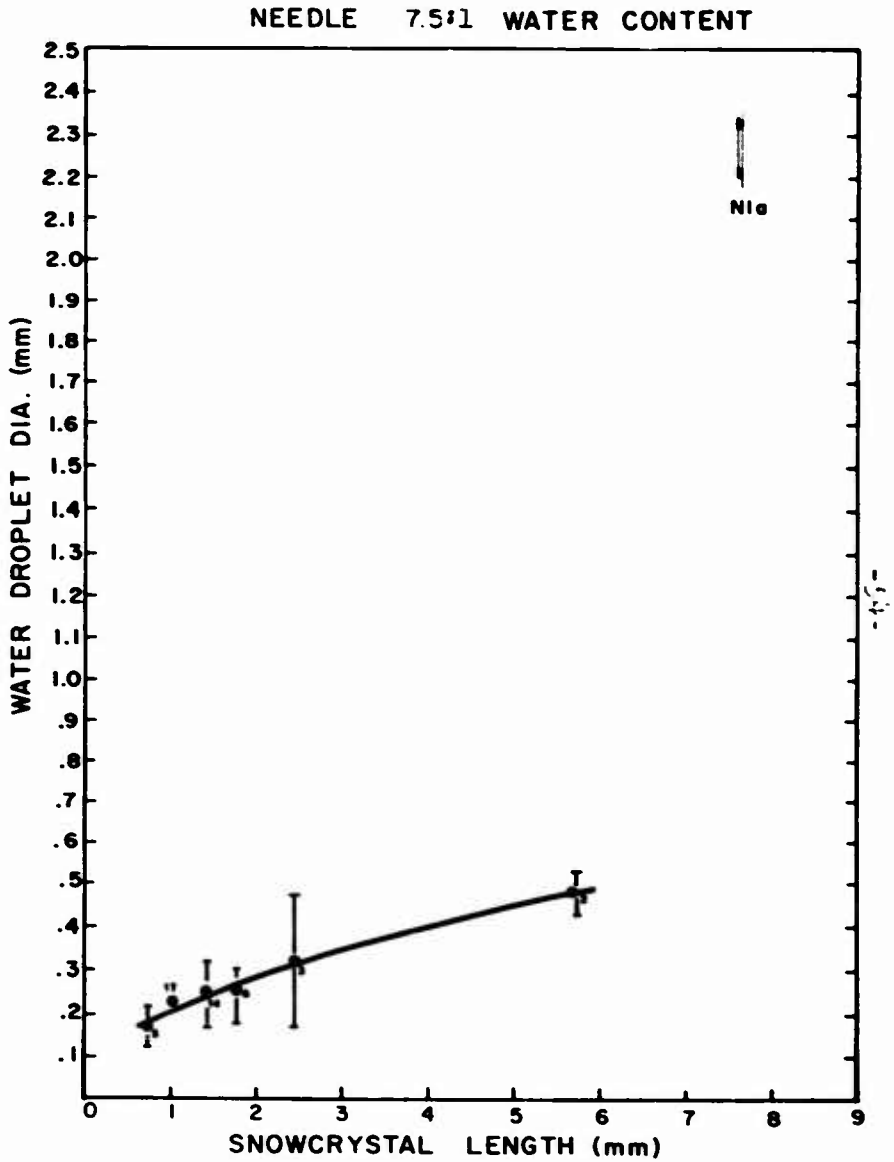

FIGURE 42

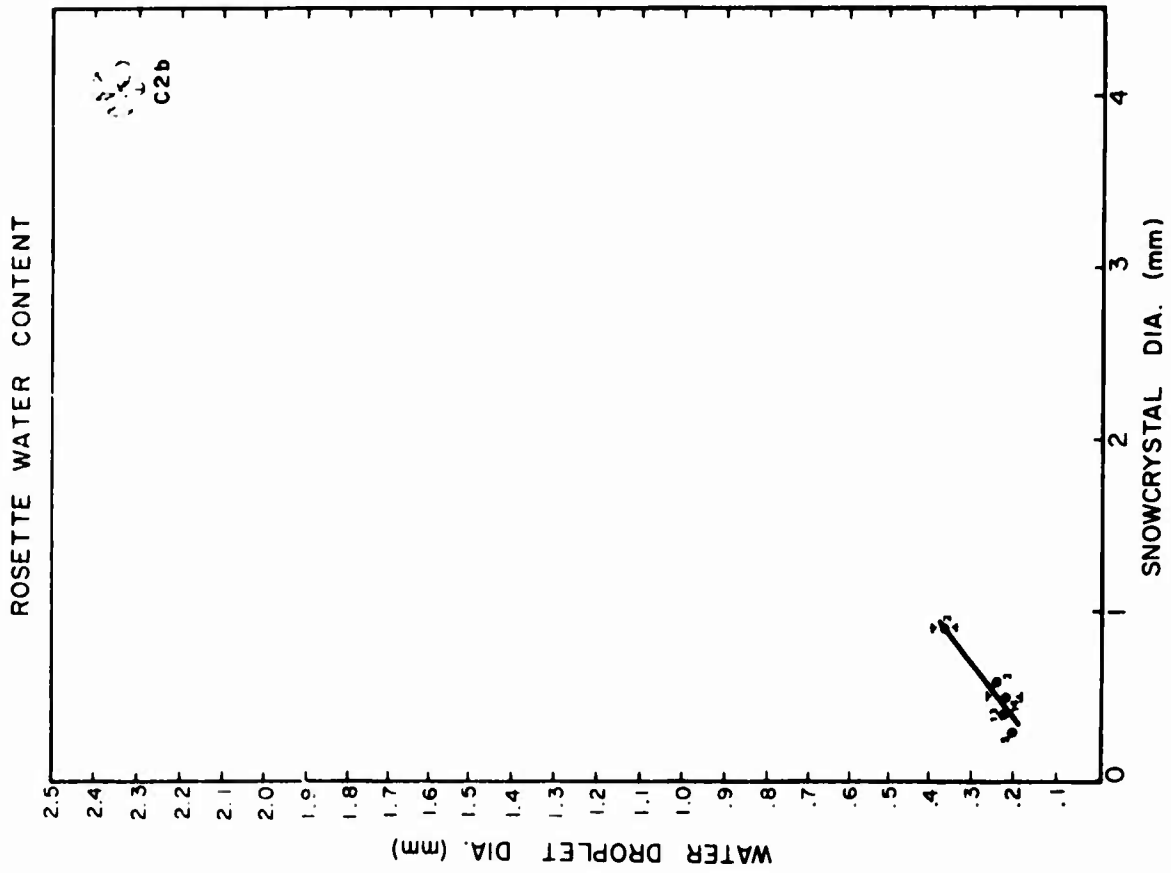

FIGURE 43

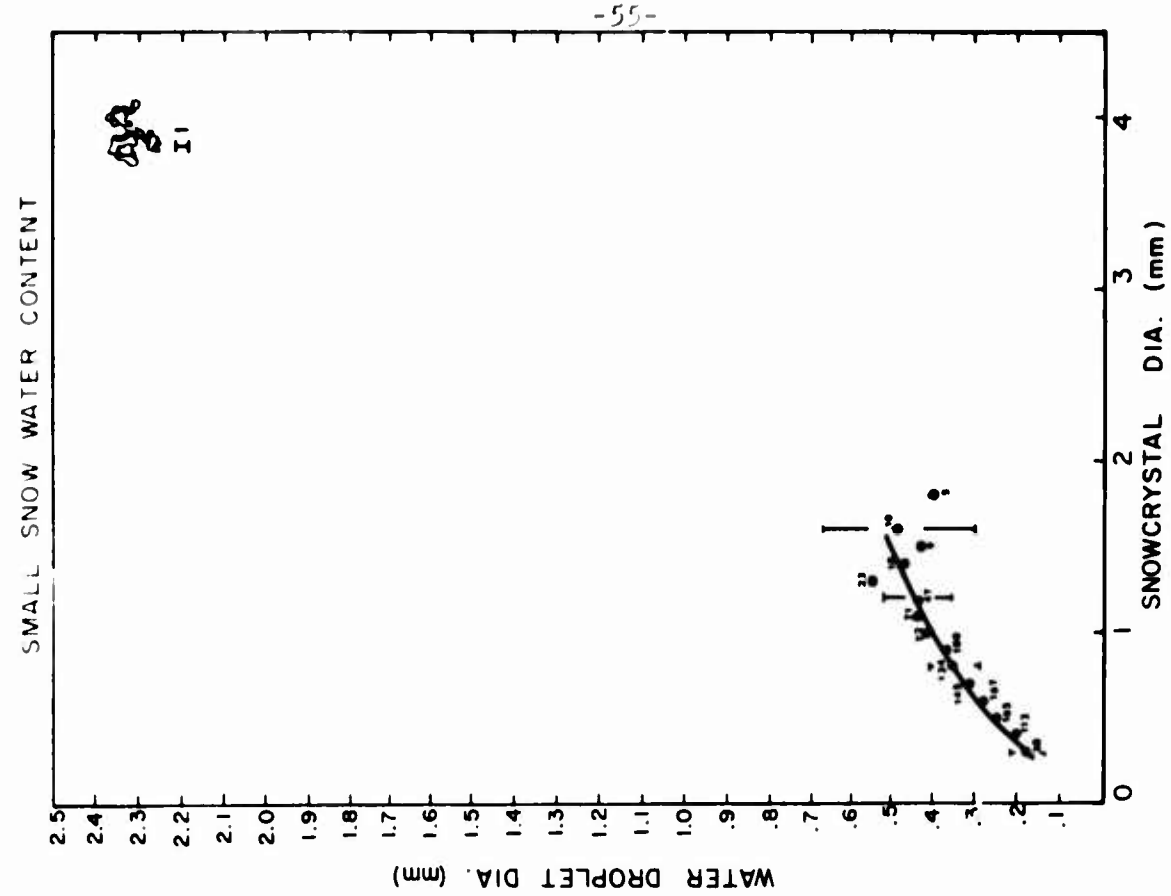

FIGURE 44

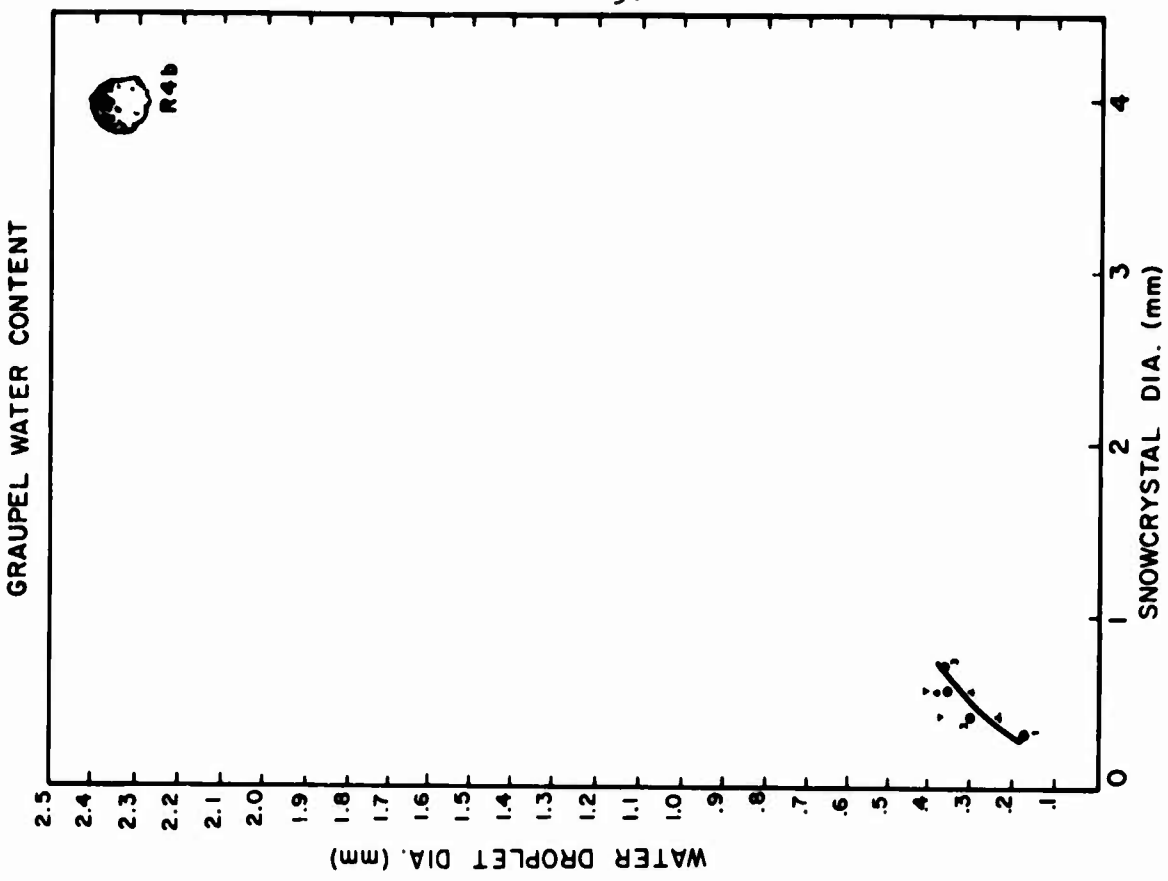

FIGURE 46

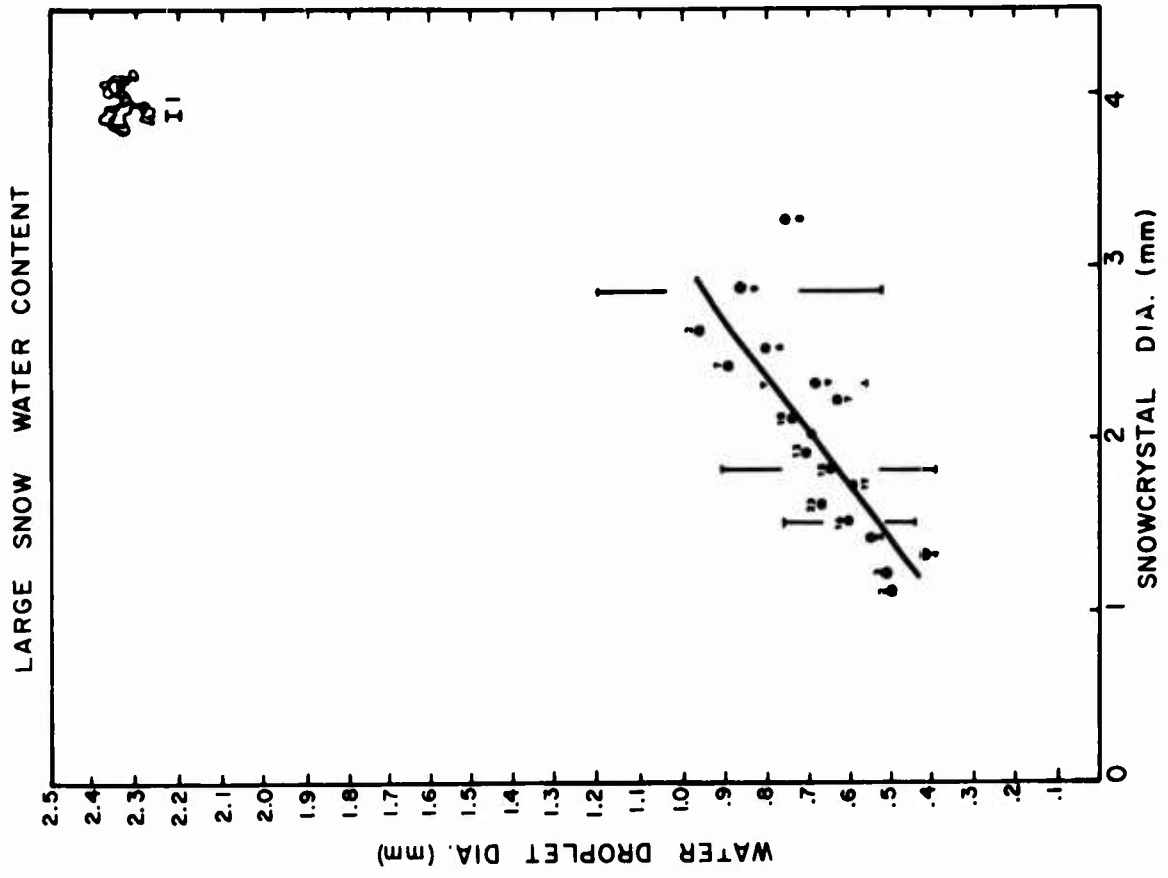

FIGURE 45

in the stellar dendrite data of Figure 39, as well as the stellar with end plate data of Figure 40. It is our opinion that these are real differences between our observations and those of others.

5.0 APPLICATION OF RESULTS

The results presented in Section 2.0 on the theoretical OAP response and that of the previous section dealing with melted diameter measurements can be used to more correctly interpret OAP measurements in snow particularly as it relates to particle mass measurements. The correct interpretation of such measurements is invaluable when direct correlations with radar (proportional to mass^2) are sought. In order to determine the melted diameters from OAP spectra, it is necessary to first determine the actual snow crystal size that corresponds to each OAP size measurement from the theoretical curves presented in Section 2. Using these corrected sizes, the melted diameter relationships presented in Section 4 can be directly applied. The difference between the actual melted diameter and those corresponding to the indicated (uncorrected) OAP snow crystal size measurements is considerable. In this section we have presented the resultant effects that probe undersizing can have on the melted diameters computed for the various snow crystal types observed, if left uncorrected. These results are presented in Figures 47-57 for the OAP-200Y precipitation probe. Similar curves can obviously be plotted for any OAP as long as the array element spacing is known.

Here, we are primarily interested in illustrating the systematic effects of undersizing and the amount of difference in undersizing between the array element geometries of Figures 1 & 2. The undersizing phenomenon is obvious in all figures. Figures 50, 52 and 53 illustrate the effect of array element geometry on the roundoff error at small sizes. Oftentimes the initial size threshold occurs at quite larger sizes. It is interesting to see that the

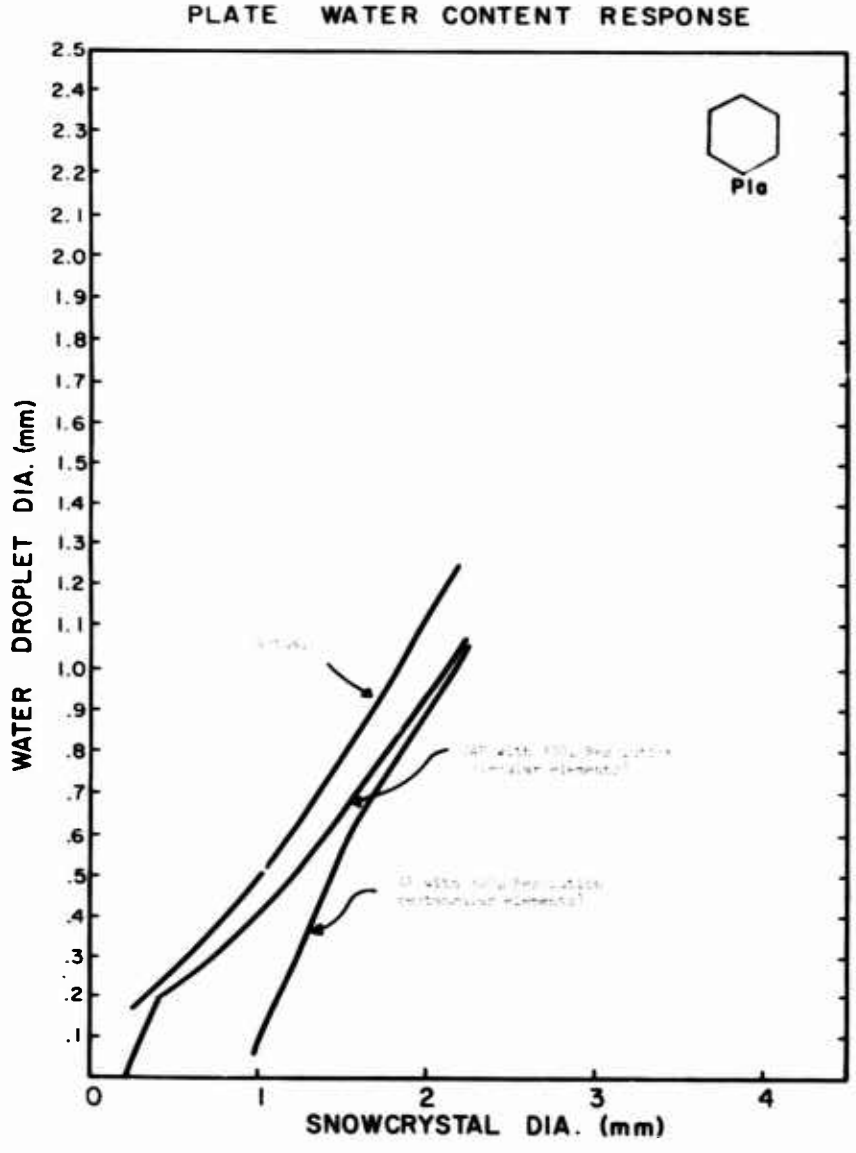

FIGURE 47

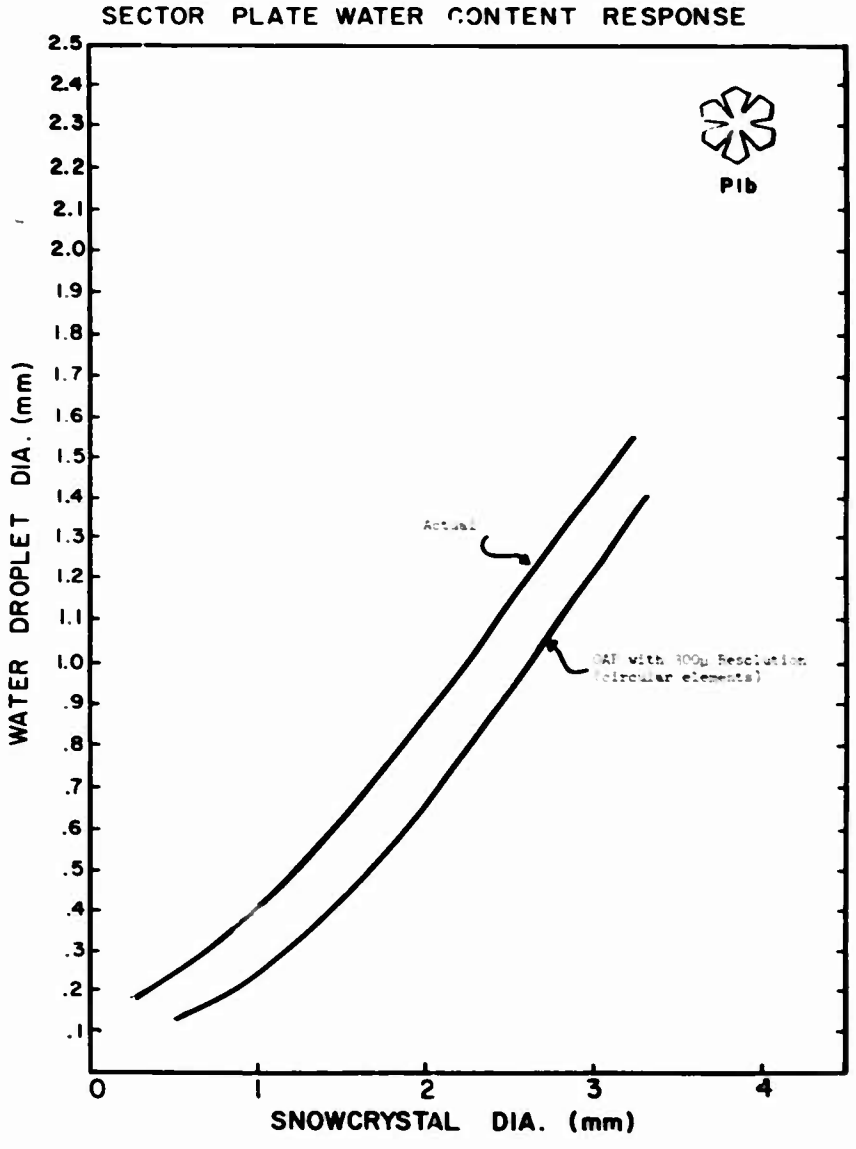

FIGURE 48

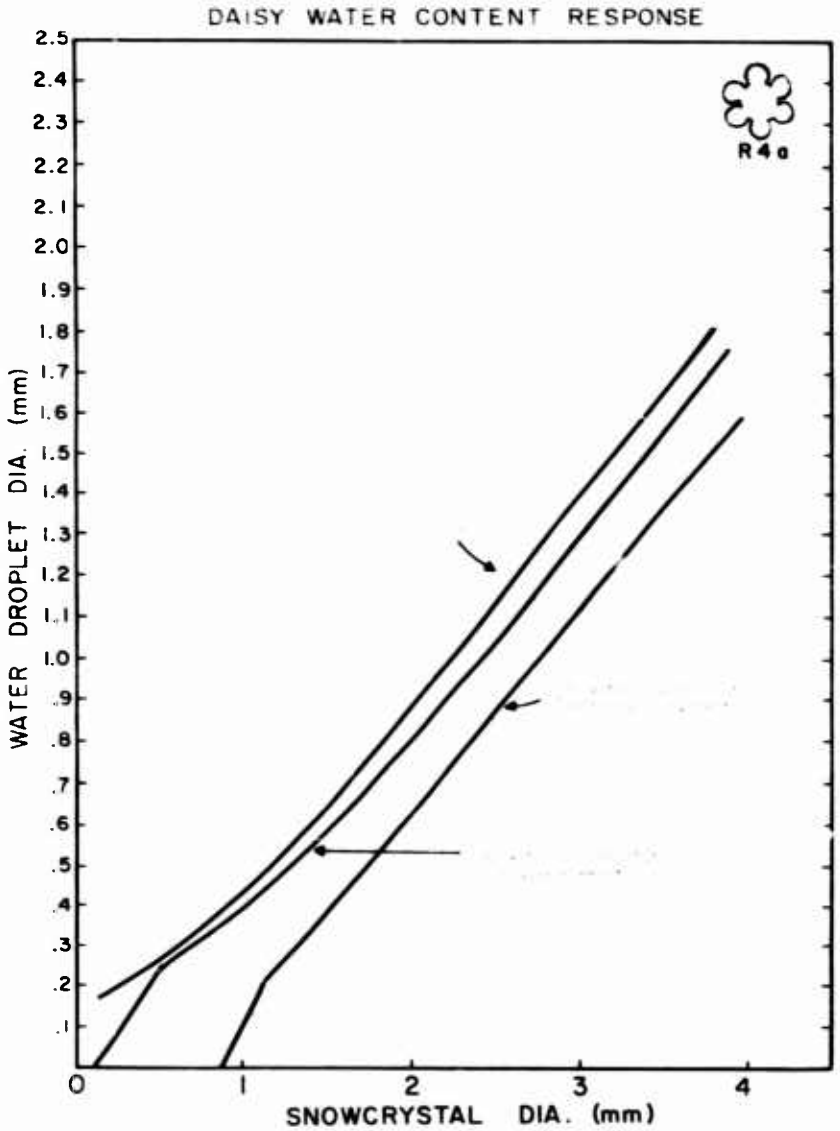

FIGURE 49

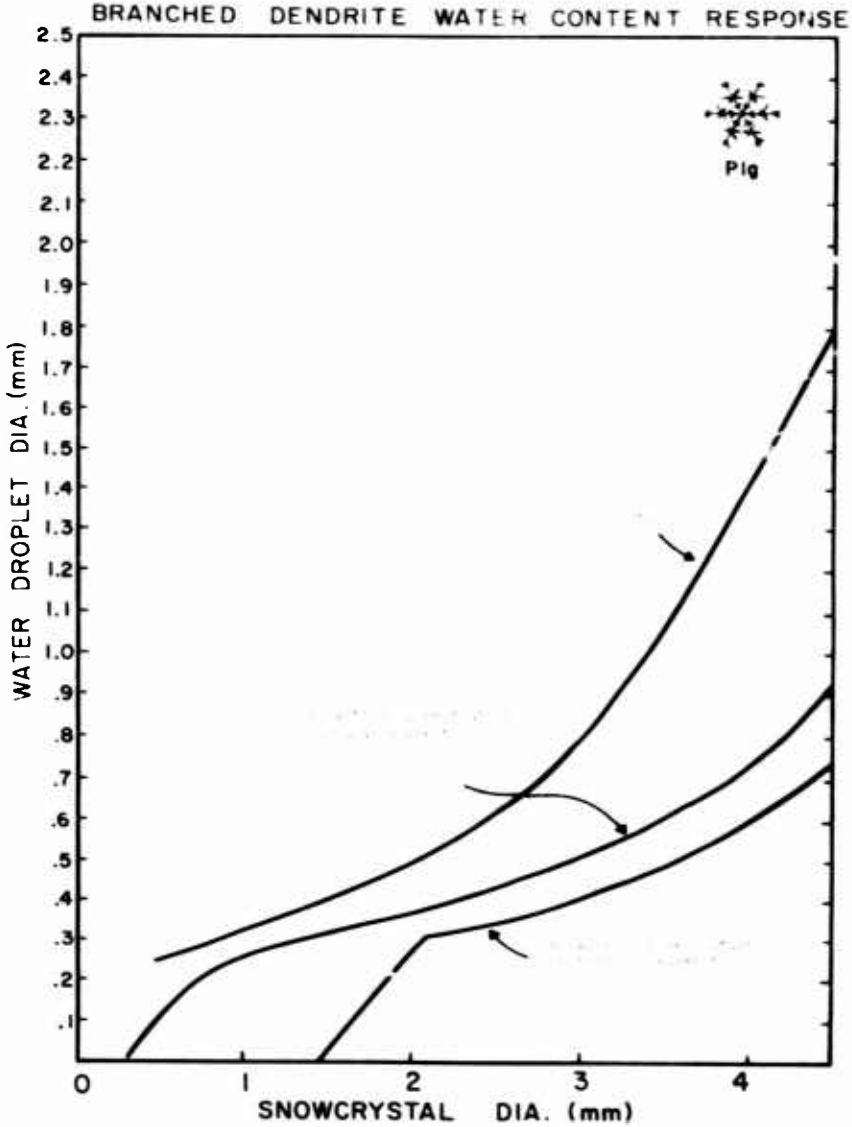

FIGURE 50

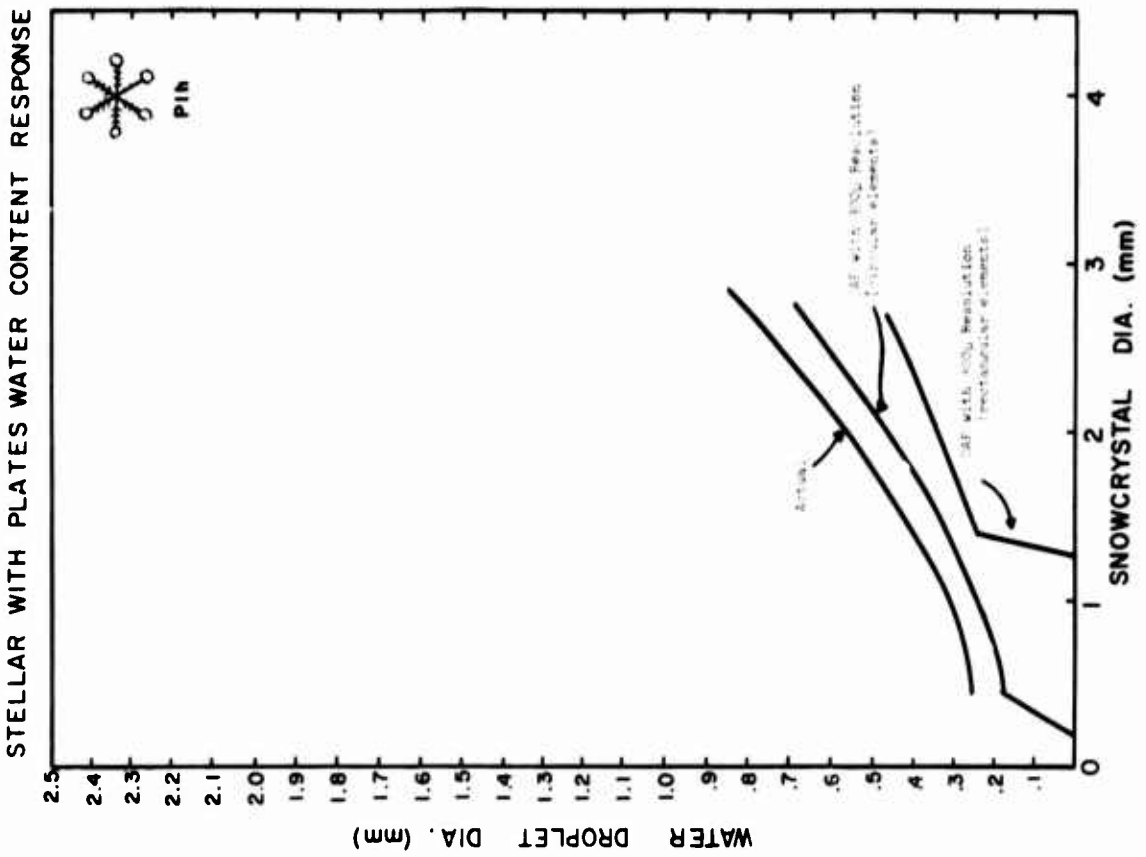

FIGURE 52

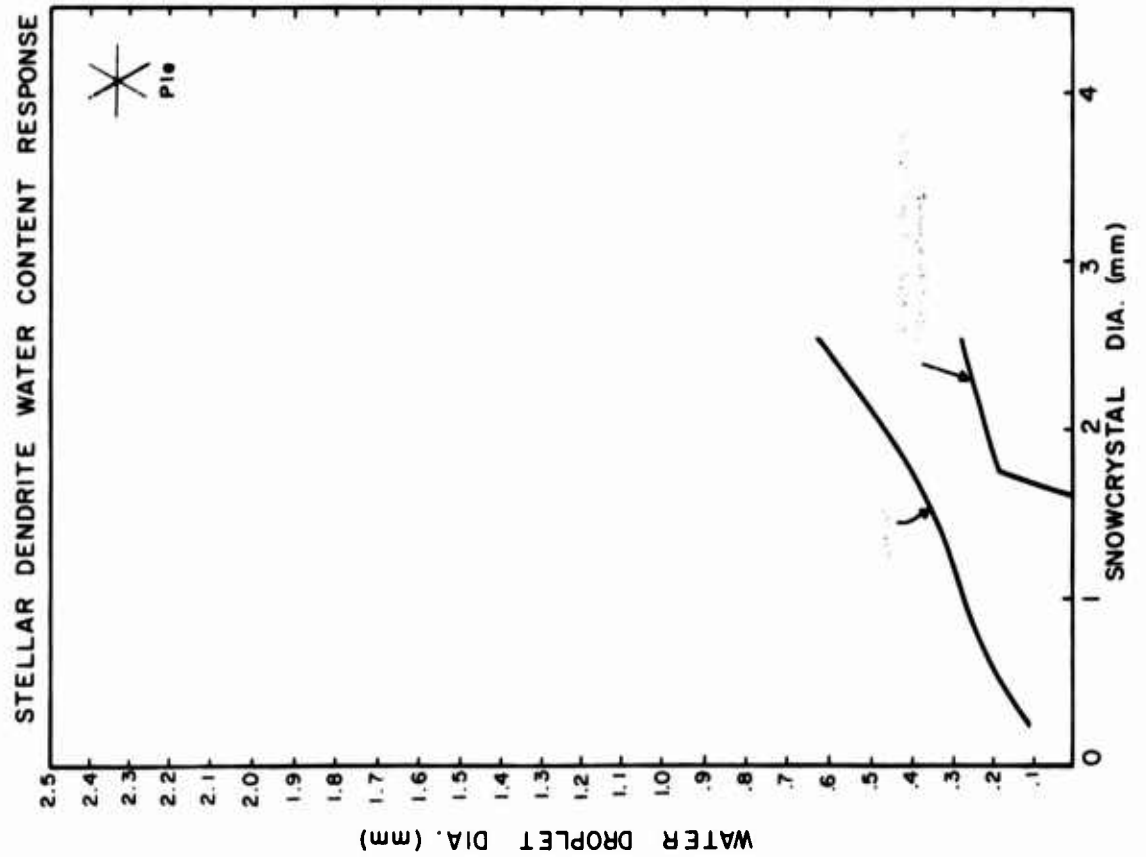

FIGURE 51

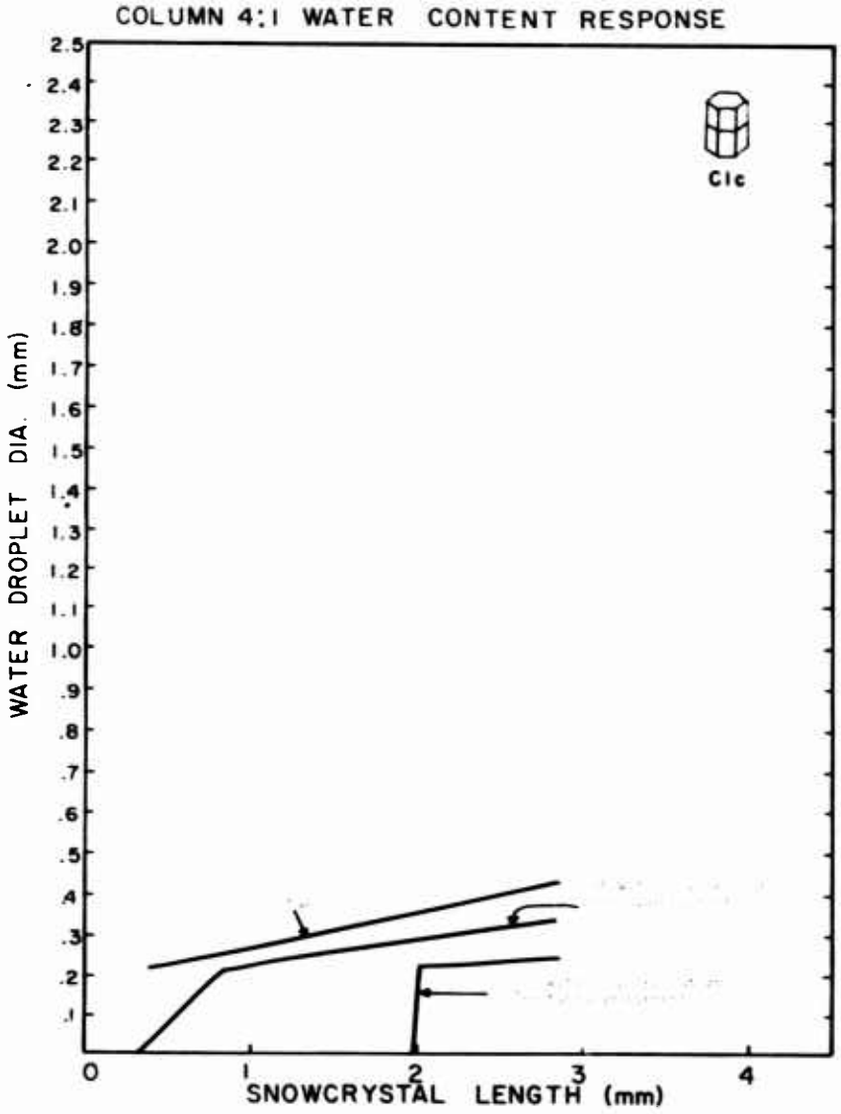

FIGURE 53

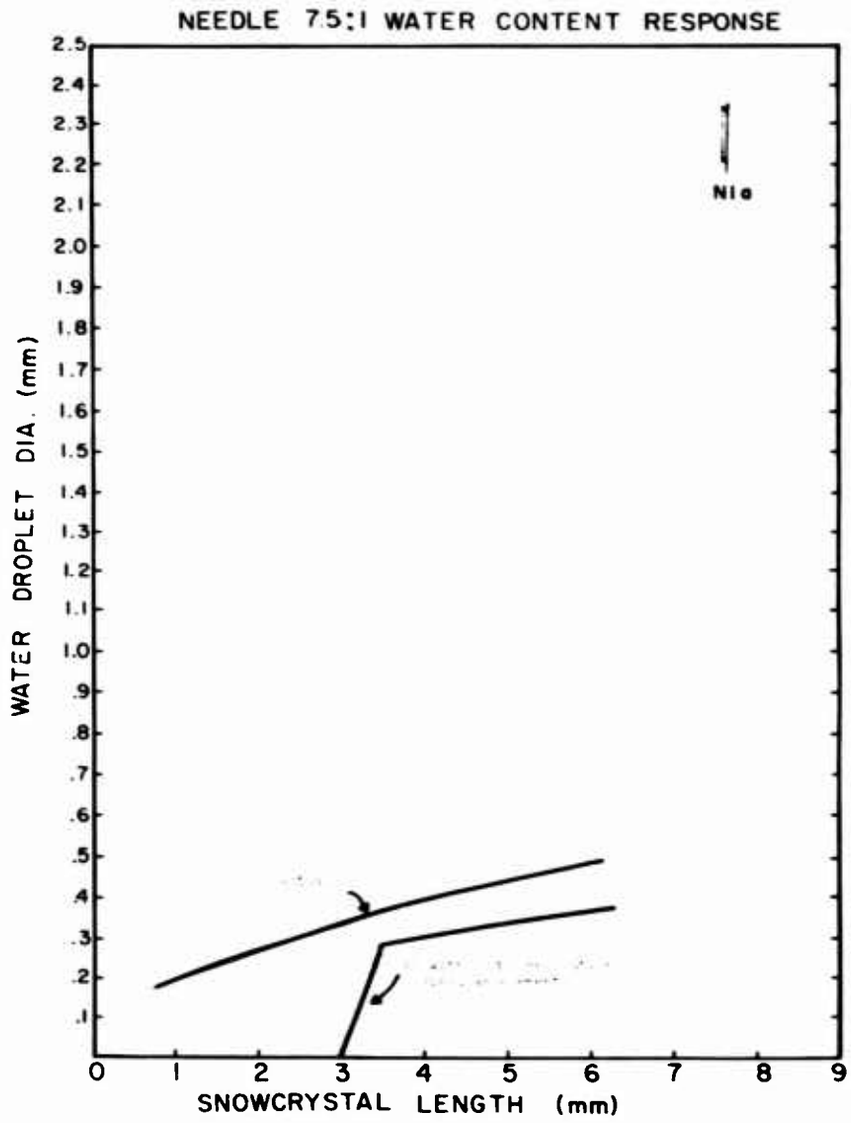

FIGURE 54

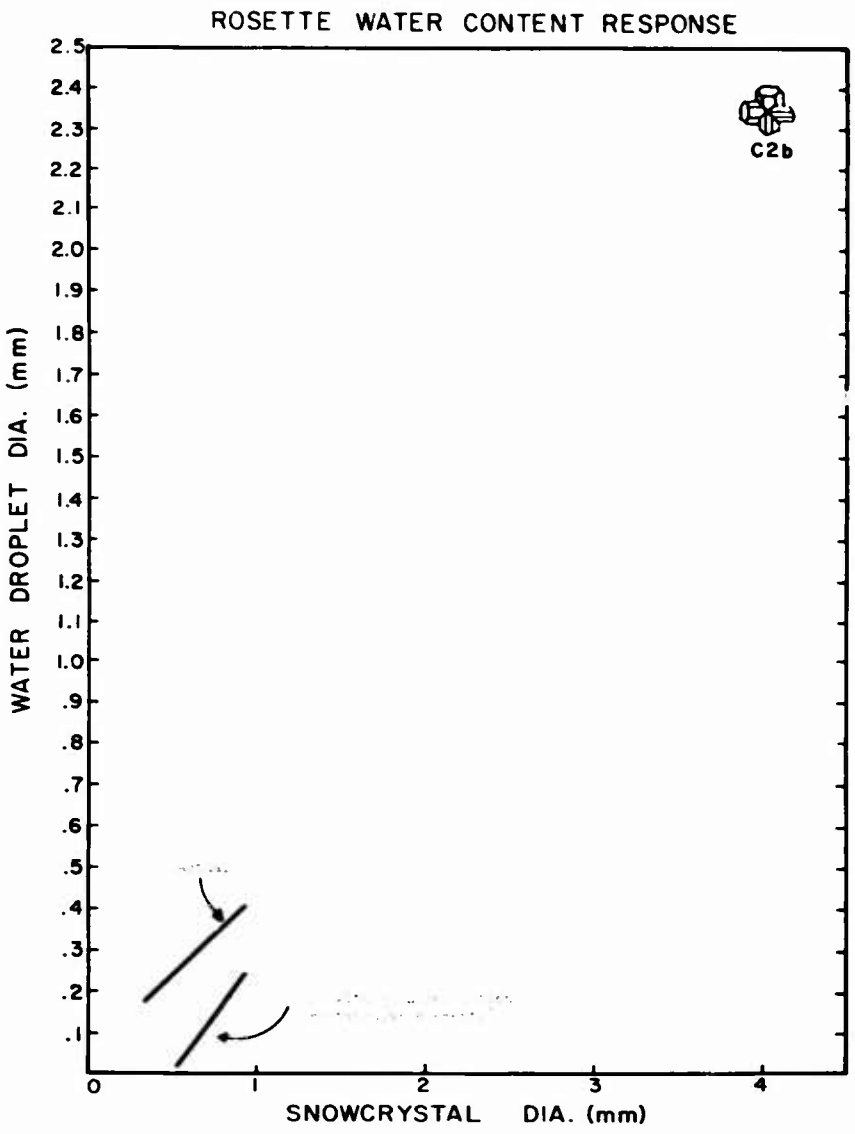

FIGURE 55

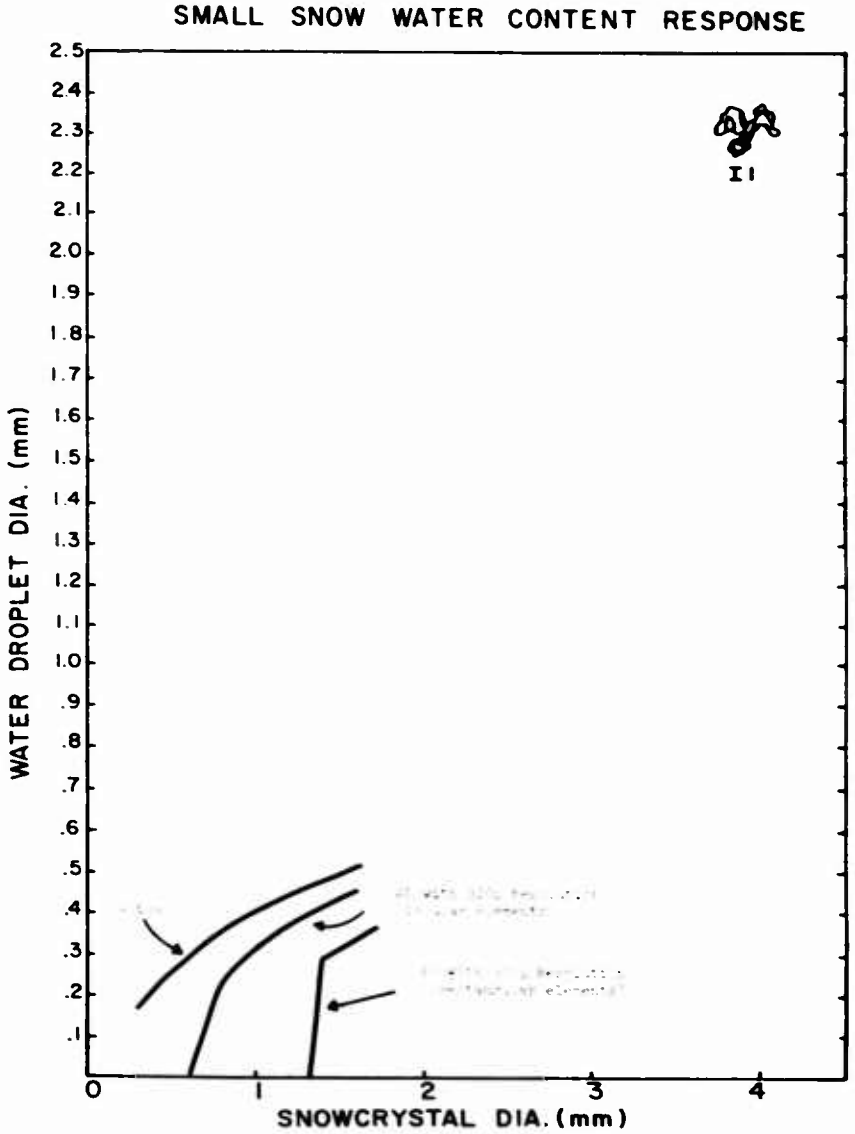

FIGURE 56

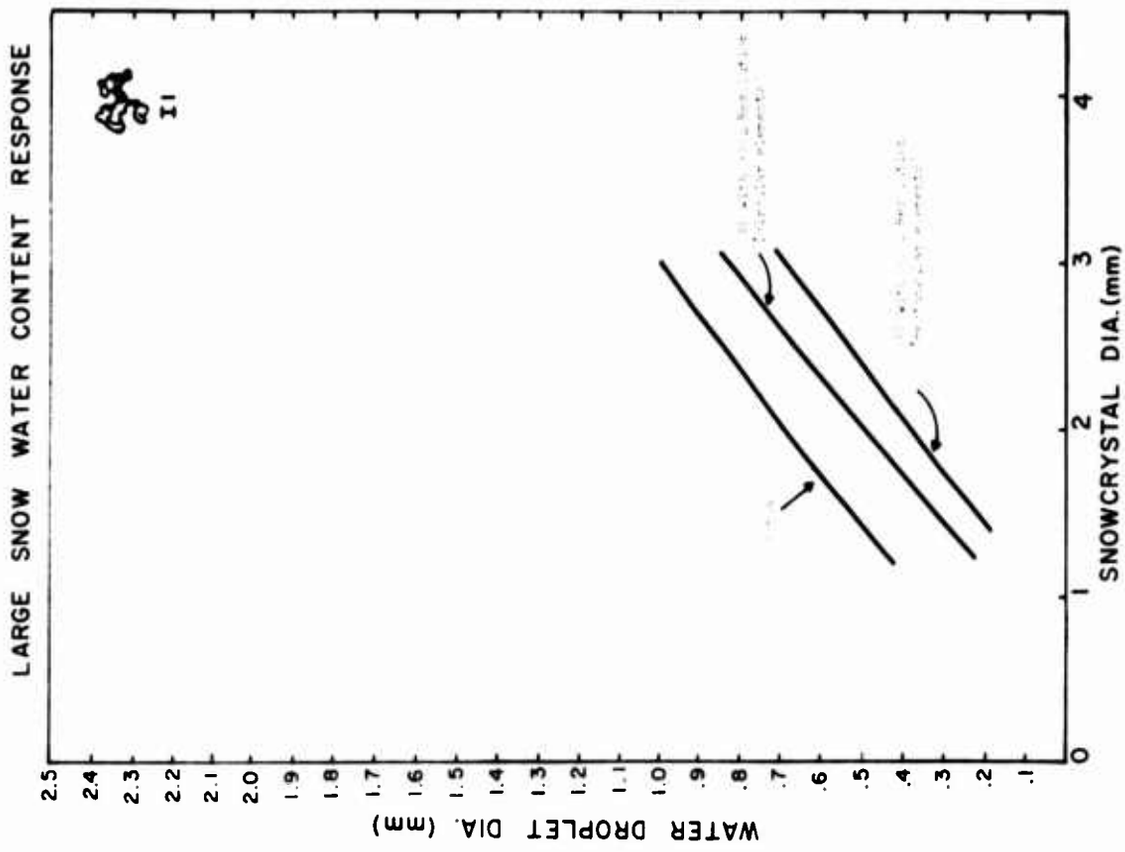
LARGE SNOW WATER CONTENT RESPONSE
I1
WATER DROPLET DIA. (mm)
SNOWCRYSTAL DIA.(mm)
0
1
2
3
4
.1
.2
.3
.4
.5
.6
.7
.8
.9
1.0
1.1
1.2
1.3
1.4
1.5
1.6
1.7
1.8
1.9
2.0
2.1
2.2
2.3
2.4
2.5

FIGURE 57

effect of array element geometry varies greatly depending on snow crystal habit. In general, the more open the structure exhibited by the crystal type, the greater the discrepancy between the two element geometries. This is easily observed by comparing Figures 52 and 56. Of course we have previously mentioned a more extreme case where the needle family is not seen with arrays of rectangular element geometry. The same is true for the size range of bullet rosettes our field data provided.

There is one particular area where caution is advised in applying the results of Section 2. Snow crystals with large aspect ratios (particularly needles, bullets and columns) have actual response functions which are stongly orientation dependent. The curves presented here are average response functions for all orientations. Previously, such data have been treated by a cascading spectral convolution starting at the largest size measured. The process removes counts from smaller channels (probe undersized counts) and adds them to larger channels to correct for orientation effects. This process is strictly more correct than using average response functions, particularly with regard to size spectral characteristics, but the difference is not significant with regard to water content. PMS can provide preferred cascading convolutions based on current theoretical results. Such cascading convolutions are unnecessary for other crystalline habits and are nearly impossible to use when there is mixed habit.

6.0 CONCLUSIONS

The results of this study show that the response of Optical Array Spectrometers follows the prediction of theoretical-empirical measurements. This is clearly evidenced by the response of 2-D spectrometers to both laboratory test models and natural snow crystals at aircraft speeds. This does not mean that the probe response is the same for "ideal" spherical particles as it is in the case of the varied particle morphology in natural snow. On the contrary, sizeable errors in particle size and particle mass systematically result with measurements in natural snow; however, the general undersizing that results in natural snow is as well predicted by the theoretical-empirical measurements.

While it is certain that the greatest error in estimating ice water content from OAP data lies in the undersizing of particles characteristic of the instrument, our field measurements of the ice water content of natural snow crystals are in general greater than that currently used in the C-130 data analysis. This is to a greater extent true in the larger sizes. For instance, our data for the general dendritic family systematically show a melted diameter relationship with an increasing positive slope at larger sizes. This is not too surprising in that the previous data in general do not extend to as large a size as ours do, and in general our data are more extensive at all sizes. When combined, the undersizing error of the probe and the greater mass we find for various crystals can account for errors as large as an order of magnitude in water content measurement if uncorrected. As far as the

C-130 operations are concerned, the general category of large snow shows systematic underestimates of melted diameter of 60% using an array with circular elements and almost a factor of two with rectangular elements. This results in an underestimate of a factor of four in ice water content for circular elements and a factor of eight for rectangular elements. It should be pointed out in general that the ice water content does not have appreciable contribution from the range of sizes measured on the OAP 200X Cloud Droplet Probe (20 - 300u). Therefore, the estimates just given refer to the 200Y Precipitation Probe (300 - 4500u). Similar errors just described dominate the dendritic family. In general, errors are least for the plate family (includes sector plates and daisy crystals). The columnar family can also result in large errors, particularly if the aspect ratio is high. In general, it must be considered that the OAP 200Y probe with rectangular elements is non responsive to needle crystals. Even with circular elements the OAP-200Y Probe cuts off at mid range and has appreciable undersizing errors in the rosette and columnar type crystals.

We feel with some certainty that data analysis using the response characteristics we have documented will greatly improve ice water content agreement between OAP's and that inferred from radar. This is particularly true with regard to measurements where the ice water content is generated by particle sizes larger than 50-60u. At the present time there is still some uncertainty with regard to the OAP 200X response at small sizes. In view of the fact that ice crystals less than 100u are not stably orientated, probably are more transparent, and their morphology, in general, the least

defined it is difficult to predict the respective undersizing at these sizes. Coupled with this, the fact that the OAP 200X Cloud Droplet Probe has a secondary depth-of-field threshold which requires a certain portion of the shadow image to approach 70% darkness levels to be accepted causes us some concern with regard to the resultant depth-of-field for these same ice crytal sizes. In addition, there is the fact that the bandwidth of the OAP 200X photodetector module is marginal for 20u sizes at speeds greater than 100 m sec^{-1}. It must be assured that the amplifiers can respond with minimum droop in approximately 0.4 microseconds (the preamp circuits in general have a peaking transfer function from 2-4MHz which includes the range of response speeds just discussed). However, even though the response time may be adequate the 70% threshold level may not be exceeded as easily for snow crystals as for spherical particles. Thus, it is probable that the depth-of-field at the small size end of the OAP 200X probe is substantially less than given. In general, the 2-D response would support a comparable depth-of-field for small ice crystal features as for comparable spherical elements at the 50% threshold (used in all 2-D probes). During the next year we will be testing a 2-D probe with multilevel thresholds that are programable, and following that, a four level gray scale instrument. These instruments should ascertain whether or not the combination of bandwidth limitation, secondary threshold settings, etc., require redefinition of the depth-of-field for small snow crystals.

Irregardless, the OAP 200Y probe which operates at the

same 50% threshold settings as the 2-D probe has no bandwidth limitation and without the secondary threshold can not produce any appreciable errors in the manner we have just discussed. Even so, we find the same apparent undersizing or undercounting at the small sizes within its range as we do with the OAP 200X probe. One may argue that since the effects are similar that they are likely similar in origin. While the argument is somewhat circular the known adequate response time and proper threshold level settings in the 200Y probe lead one to suspect that these parameters similarly may be adequate in the OAP 200X probe. However, the effect of the secondary threshold in the OAP 200X probe can not be overlooked. It is our opinion that the similar undersizing/undercounting properties that exist for the two probes are really caused by different particle parameters and probe characteristics. We believe that the OAP 200Y probe's undersizing/undercounting effects are almost entirely induced by particle morphological features, and thus with proper knowledge of snow crystal habit are resolvable. In the case of the OAP 200X probe the variations with particle morphology are substantially reduced in the size range where the apparent undersizing/undercounting phenomenon is observed. While we can not be absolutely sure until complete measurements are made at reduced thresholds, it is our current opinion that we are losing depth-of-field and undercounting particles in this small end of the OAP 200X size range. Recent experiments (see Section 3.3) have confirmed that even in the case of spherical elements the sample area is reduced below given values for size channels 1, 2 and 3. The depth-of-field generally extends to the given limits; however, because of the secondary depth-of-field threshold the "capture" or sample probability is less than 100%. The sample probabilities for size channels 1, 2 and 3 are 25%, 62% and 89% respectively. These values may still be too high for certain small snow crystals.

REFERENCES

Knollenberg, R. G. and W. E. Neish, 1969: "A New Electro-Optical Technique for Particle Size Measurements", Proc. Electro-Optical Sys. Design Conf., PP. 594-608

Knollenberg, R. G.,1970: "The Optical Array: An Alternative to Extinction and Scattering for Particle Size Measurements", J. Appl. Meteor.,Vol 9, No. 1, PP. 86-103

Knollenberg, R. G.,1972: "Comparative Liquid Water Content Measurements of Conventional Instruments with an Optical-Array Spectrometer", J. Appl. Meteor.,Vol 2, No. 3, PP.501-508

Magono, C. and C. W. Lee, 1966: Meteorological Classification of Natural Snow Crystals, J. Fac. Sci. Hokkaido Univ. Ser. 7, 2, 320-335